# TECHNICAL NOTE

D-1947

# TRANSONIC INVESTIGATION OF THE STATIC LONGITUDINAL AERODYNAMIC CHARACTERISTICS OF LOW-ASPECT-RATIO WING-BODY CONFIGURATIONS AT ANGLES OF ATTACK FROM $0^{o}$ TO $90^{o}$

By Charles D. Trescot, Jr., Lawrence E. Putnam,
and Cuyler W. Brooks, Jr.

Langley Research Center
Langley Station, Hampton, Va.

NATIONAL AERONAUTICS AND SPACE ADMINISTRATION
WASHINGTON

June 1963

NATIONAL AERONAUTICS AND SPACE ADMINISTRATION

TECHNICAL NOTE D-1947

# TRANSONIC INVESTIGATION OF THE STATIC LONGITUDINAL AERODYNAMIC CHARACTERISTICS OF LOW-ASPECT-RATIO WING-BODY CONFIGURATIONS AT ANGLES OF ATTACK FROM 0° TO 90°

By Charles D. Trescot, Jr., Lawrence E. Putnam, and Cuyler W. Brooks, Jr.

## SUMMARY

An investigation has been conducted in the Langley transonic blowdown tunnel to determine the effects of wing planform and other geometric parameters on the static longitudinal aerodynamic characteristics of winged vehicles suitable for reentry. Wing leading-edge radius and wing lower surface contour were also varied for several of the configurations during the investigation. The tests were made at Mach numbers of about 0.8, 1.01, and 1.18 for angles of attack that generally varied from about -4° to 91°.

The results of the investigation indicate that, at a given test Mach number, planform variation for the basic models had a considerable effect on lift-curve slope at an angle of attack of 0° but had essentially no effect on maximum lift coefficient, lift-curve slope at an angle of attack of 90°, or maximum drag coefficient. The values of maximum lift-drag ratio for the circle model varied between 2.5 and 3.0 whereas those of the other basic planforms generally varied between 3 and 4. The basic planforms were longitudinally unstable below the angle of attack at which maximum lift was obtained and longitudinally stable above this angle of attack, the moment reference point being located at the centroid of planform area of each planform. Changing the leading edge of the 65° triangular model from cylindrical to square caused higher maximum drag and, generally, small positive increments in pitching moment through the test angle-of-attack range. Contouring the wing lower surface of the basic ellipse model to form the model designated as ellipse (convex) caused positive increments in pitching moment, decreases in lift coefficient and maximum drag coefficient, and small changes in stability. Contouring the wing lower surface of the 75° model to form a trihedron model caused large negative increments in pitching-moment coefficient, an increase in lift coefficient below and a decrease in lift coefficient above an angle of attack of 20°, and an increase in drag coefficient below an angle of attack of about 50°. The trihedron model had the lowest maximum lift-drag ratio of the configurations tested.

## INTRODUCTION

The National Aeronautics and Space Administration is investigating the effects of wing planform and other geometric parameters on the aerodynamic stability and control of winged reentry vehicles. The knowledge being obtained will be applicable to vehicle design and evaluation of reentry concepts. One concept for winged reentry vehicles utilizes lift up to the maximum during the reentry phase. Another concept for these vehicles utilizes high drag, obtained at an angle of attack near 90°, during the reentry phase. In this latter concept, the angle of attack is not reduced to provide relatively high performance until either subsonic or moderate supersonic speeds are reached. (See ref. 1.) The investigations, therefore, are usually being made at angles of attack from approximately 0° to 90° and speeds from subsonic to hypersonic.

The purpose of this paper is to show the effects of wing planform and other geometric parameters on the longitudinal aerodynamic characteristics of a series of winged reentry vehicles at transonic speeds. These transonic test results were obtained on configurations with six different wing planforms. Wing leading-edge radius and airfoil section lower surface contour were also varied in the investigation. The tests were made at Mach numbers of about 0.80, 1.01, and 1.18 for angles of attack that were generally varied from -4° to 91°. Reynolds number, based on the wing mean aerodynamic chord, varied from $2.37 \times 10^6$ at a Mach number of 0.80 to $3.77 \times 10^6$ at a Mach number of 1.18. Results showing effects of somewhat similar planform variations at supersonic speeds are available in references 2 and 3. Results at hypersonic speeds showing the effect of planform variations identical to those of the present investigation are available in reference 4.

## SYMBOLS

The force and moments are referenced to the stability axes which have their origin on the body center line and at the centroid of area of the model planform. All coefficients for a given wing planform are based upon the mean aerodynamic chord and planform area of that wing.

| | |
|---|---|
| $A$ | aspect ratio, $\frac{b^2}{S}$ |
| $b$ | wing span |
| $C_A$ | axial-force coefficient, $\frac{\text{Axial force}}{q_\infty S}$ |
| $C_D$ | drag coefficient, $\frac{\text{Drag}}{q_\infty S}$ |
| $C_{D,max}$ | maximum drag coefficient |

$C_{D,min}$ minimum drag coefficient

$C_L$ lift coefficient, $\frac{\text{Lift}}{q_\infty S}$

$C_{L,max}$ maximum lift coefficient

$C_{L_\alpha,0^\circ} = \frac{\partial C_L}{\partial \alpha}$ per degree at $\alpha = 0^\circ$

$C_{L_\alpha,90^\circ} = \frac{\partial C_L}{\partial \alpha}$ per degree at $\alpha = 90^\circ$

$C_m$ pitching-moment coefficient, $\frac{\text{Pitching moment}}{q_\infty S \bar{c}}$

$C_m/C_N$ center-of-pressure location

$C_N$ normal-force coefficient, $\frac{\text{Normal force}}{q_\infty S}$

$C_{p,b}$ base-pressure coefficient, $\frac{p_b - p_\infty}{q_\infty}$

$\bar{c}$ mean aerodynamic chord

$h$ height

$L/D$ lift-drag ratio

$(L/D)_{max}$ maximum lift-drag ratio

$M_\infty$ free-stream Mach number

$p_b$ base pressure

$p_\infty$ free-stream static pressure

$q_\infty$ free-stream dynamic pressure

$R$ Reynolds number based on $\bar{c}$

$r$ radius

| | |
|---|---|
| $S$ | total wing area |
| $t$ | wing thickness |
| $x_{mc}$ | distance to moment center from leading edge of wing root chord |
| $l$ | length |
| $\alpha$ | angle of attack |
| $\lambda$ | taper ratio, defined as ratio of tip chord to theoretical root chord |

Subscripts:

| | |
|---|---|
| 1,2,3,4 | denote various lengths on models (see fig. 1) |

## MODELS

Drawings of the models with corresponding tables presenting pertinent dimensions are presented in figure 1 and photographs of the models are shown as figure 2. Table I presents several additional geometric parameters for each configuration that are not presented in figure 1. The basic planforms of the

TABLE I.- ADDITIONAL MODEL GEOMETRIC PARAMETERS

(a) Large models

| Model | A | $\bar{c}$, in. | S, sq in. | Moment center, percent $\bar{c}$ |
|---|---|---|---|---|
| Circle | 1.28 | 3.74 | 15.26 | 50 |
| Ellipse | 0.64 | 5.25 | 15.19 | 49 |
| Ellipse (convex) | 0.64 | 5.25 | 15.19 | 49 |
| 65° swept delta | 1.52 | 3.77 | 14.65 | 50 |
| 65° swept delta (square leading edge) | 1.52 | 3.77 | 14.65 | 50 |
| 65° swept delta (clipped) | 1.16 | 3.99 | 14.75 | 50 |
| 75° swept delta | 0.96 | 4.75 | 14.33 | 50 |
| Trihedron | 1.13 | 4.64 | 14.56 | 50 |
| 75° swept delta (clipped) | 0.70 | 5.02 | 14.45 | 50 |

(b) Small models

| Model | A | $\bar{c}$, in. | S, sq in. | Moment center, percent $\bar{c}$ |
|---|---|---|---|---|
| Circle | 1.28 | 2.54 | 7.05 | 50 |
| Ellipse | 0.64 | 3.57 | 7.02 | 49 |
| Ellipse (convex) | 0.64 | 3.57 | 7.02 | 49 |
| 65° swept delta | 1.52 | 2.56 | 6.77 | 50 |
| 65° swept delta (square leading edge) | 1.52 | 2.56 | 6.77 | 50 |
| 65° swept delta (clipped) | 1.16 | 2.71 | 6.82 | 50 |
| 75° swept delta | 0.96 | 3.23 | 6.62 | 50 |
| Trihedron | 1.13 | 3.15 | 6.73 | 50 |
| 75° swept delta (clipped) | 0.70 | 3.41 | 6.68 | 50 |

investigation are presented in figure 1(a) and consist of a circle, an ellipse, a 65° swept delta, a 65° swept clipped-tip delta ($\lambda = 0.248$), a 75° swept delta, and a 75° swept clipped-tip delta ($\lambda = 0.238$). Two sizes of models, for reasons subsequently discussed under "Apparatus and Tests," were required. The large- and small-size basic models had flat-plate wings which were 0.183 and 0.125 inch thick, respectively, with cylindrical leading edges. The cylindrical leading edges had radii of 0.091 inch and 0.062 inch normal to the wing leading edge for the large and small models, respectively. All models had identical half conical noses and similar cylindrical afterbodies which varied in length with each model. (See fig. 1(b).) These cone-cylinder bodies were mounted on the upper wing surface.

In addition to the six basic models, a 65° swept delta flat-plate wing model with a square-wing leading edge and an ellipse model (fig. 1(c)) with a contoured wing lower surface were investigated. Also tested was a trihedron model which had a 75° swept right-triangular pyramidal wing. The upper wing surface was flat and the lower wing surface had a dihedral angle of 45°. (See fig. 1(d).)

## APPARATUS AND TESTS

The tests were made in the Langley transonic blowdown tunnel which has a slotted octagonal test section measuring 26 inches between flats. The models were mounted on internal strain-gage balances which were sting-supported in the tunnel. Two balances were employed for the present tests. For the low angle-of-attack range ($\alpha \approx -3.6°$ to 46°), one of the balances was mounted in the model fuselage and extended from the base of the model. (See fig. 2(b).) The other balance was used for the high angle-of-attack range ($\alpha \approx 50°$ to 91°) and was mounted on the top of the model at an angle of 70° with respect to the body center line. (See fig. 2(d).) Force and moment data were recorded by self-balancing potentiometers on pen-type strip charts. The pressures necessary to determine dynamic pressure and Mach number and the balance cavity pressures in the low angle-of-attack range were recorded with quick-response flight-type recorders.

The tests were made at Mach numbers of about 0.8, 1.01, and 1.18 through an angle-of-attack range from about -3.6° to 91°. Reynolds number, based on the wing mean aerodynamic chord, varied from $2.37 \times 10^6$ for the circle model at a Mach number of 0.80 to $3.77 \times 10^6$ for the ellipse model at a Mach number of 1.18.

For all tests, transition strips consisting of 0.001- to 0.002-inch carborundum grains were attached to the model configurations. The grain size, which was selected after a study of reference 5, was approximately the minimum size required to cause boundary-layer transition. The strips were about 1/16 of an inch wide and the grains covered 5 to 10 percent of the strip area. The leading edges of the transition strip were located on the upper and lower surfaces of the wing at 5 percent of the local chord, and on the body at the line of tangency between the spherical nose and the forebody cone.

In order to minimize the effects of tunnel blockage on the model aerodynamic characteristics at angles of attack above about 50°, smaller models than those

used in the low angle-of-attack range (-3.6° to 46°) were utilized. The models tested at the higher angles of attack were 0.68-scale models of those tested at the lower angles of attack; thus a decrease in the ratio of model wing planform area to test-section cross-sectional area from 0.0262 to 0.0121 results. The small models were tested at an increased tunnel stagnation pressure so that the Reynolds number (based on mean aerodynamic chord) would be comparable for both model sizes.

## ACCURACY AND CORRECTIONS

The accuracy of the aerodynamic coefficients, based on estimated balance precision, is believed to be within the following limits:

| | |
|---|---|
| At $\alpha$ = -4° to 45°: | |
| $C_N$ | ±0.01 |
| $C_A$ | ±0.002 |
| $C_L$ | ±0.01 |
| $C_D$ at $\alpha$ = 0° | ±0.002 |
| $C_D$ at $\alpha$ = 45° | ±0.009 |
| $C_m$ | ±0.003 |
| At $\alpha$ = 50° to 91°: | |
| $C_N$ | ±0.02 |
| $C_A$ | ±0.01 |
| $C_L$ | ±0.02 |
| $C_D$ | ±0.02 |
| $C_m$ | ±0.004 |

Accuracy of base-pressure coefficient, Mach number, and angle of attack is believed to be within the following limits:

| | |
|---|---|
| $C_{p,b}$ | ±0.005 |
| $M_\infty$ | ±0.02 |
| $\alpha$, deg | ±0.1 |

The results of the investigation have not been corrected for the effects of either tunnel-wall or sting interference, nor has the drag data been adjusted to a condition of free-stream static pressure at the model base. The effect of Mach number on the variation of base-pressure coefficient with angle of attack is presented in figure 3 for the various configurations. The angles of attack have been corrected for sting and balance deflections due to aerodynamic loads.

In order to show possible tunnel-wall effects on the data, a comparison of the aerodynamic characteristics of the large and small 65° configurations is presented in figure 4 for high angles of attack where tunnel-wall effects are

believed to be a maximum. On the basis of this comparison, the tunnel-wall effects appear to be small and within data repeatability.

## STING INTERFERENCE EFFECTS

An examination of the lift and drag data of figures 5 to 13 shows that discontinuities exist between the data obtained with the base-mounted support and the top-mounted support at angles of attack near 50°. To provide an indication of the magnitude of the sting effects in this intermediate angle-of-attack range, additional tests were made at each test Mach number. Measurements were made on one of the top-mounted models at an angle of attack of about 52° with the base sting in its normal position with respect to but not touching the model, and also with the base sting removed from the tunnel. Measurements were likewise made on one of the base-mounted models at an angle of attack of about 46° with the top-mounted support in its normal position with respect to but not touching the model, and also with the top-mounted support removed from the tunnel.

At all test Mach numbers, the base-mounted support caused increases in $C_N$ whereas the top-mounted support caused reductions in $C_N$ in this intermediate range of angle of attack, a result consistent with the discontinuities shown. The effects on $C_A$ and $C_m$ of each support were generally within the estimated balance accuracy. The lift and drag curves of figures 5 to 13, therefore, have been faired so as to compensate partially for these sting interference effects. The differences between the faired curves and the data points are not sufficiently large to influence the fairing of the lift-drag ratio curves.

## PRESENTATION OF RESULTS

The basic longitudinal aerodynamic characteristics of the circle, ellipse, ellipse (convex), 65° swept delta, 65° swept delta (square leading edge), 65° swept delta (clipped tip), 75° swept delta, 75° swept delta (clipped tip), and trihedron models are presented in figures 5 to 13, respectively. On each of these figures, the variations of pitching-moment coefficient, lift coefficient, drag coefficient, and lift-drag ratio with angle of attack are presented at Mach numbers of about 0.80, 1.01, and 1.18.

The effects of Mach number on minimum drag coefficient, lift-curve slope at an angle of attack of 0°, and maximum lift-drag ratio are shown in figure 14 and the effects of Mach number on maximum drag coefficient, lift-curve slope at an angle of attack of 90°, and maximum lift coefficient are shown in figure 15. The effect of Mach number on the variation of center of pressure with angle of attack for each configuration is presented in figure 16. For comparative purposes, the pitching-moment curves of the basic data figures (figs. 5 to 13) have been replotted without symbols as figure 17.

## DISCUSSION

### Effect of Planform Variation

In order to minimize the effects of the body on the comparative aerodynamic characteristics of the various planform shapes, the ratio of maximum body cross-sectional area to wing planform area was held essentially constant for all models.

As would be expected, the lift-curve slope at an angle of attack of 0° of the six basic planforms (fig. 14) increased with aspect ratio; the increases were in the following order: the ellipse, the 75° clipped, the 75°, the 65° clipped, the circle, and the 65°. (See table I.) Planform variation generally had little effect on the values of lift-curve slope at an angle of attack of 90° or on maximum lift coefficient. (See fig. 15.)

The values of minimum drag coefficient for the six basic configurations generally vary directly with the configuration frontal area at each test Mach number. (See fig. 14.) The decrease in $C_{D,min}$ with an increase in Mach number from 1.01 to 1.18 for the four basic triangular planforms is large compared with that for the ellipse and circle models and is associated with the favorable effect of leading-edge sweep on pressure drag. At a given test Mach number, the effect of planform variation on the values of maximum drag coefficient for the six basic configurations was small. (See fig. 15.) The values of $C_{D,max}$ for these models occurred at or near an angle of attack of 90° where the models act essentially as flat plates.

The values of maximum lift-drag ratios for the triangular-shaped models (65°, 65° clipped, 75°, and 75° clipped) generally varied between about 3 and 4 throughout the test Mach number range. (See fig. 14.) The ellipse model had values of $(L/D)_{max}$ slightly lower than those of the triangular models at Mach numbers of 1.01 and 1.18 whereas the values of $(L/D)_{max}$ for the circle model varied between about 2.5 and 3.0 and were the lowest of the six basic configurations. The maximum lift-drag ratios of the six basic configurations occurred at angles of attack from about 8° to 13°. (See figs. 5, 6, 8, and 10 to 12.)

The pitching-moment curves for the basic planforms indicate that all of the configurations were unstable at angles of attack up to maximum lift for the moment center located at the wing centroid of area. (See figs. 5, 6, 8, and 10 to 12.) Above these angles of attack, the configurations became longitudinally stable. As shown in figure 17(a), increasing sweep from 65° to 75° at a Mach number of 0.80 reduced the instability at angles of attack up to about 30° and caused the angle of attack at which the configuration became stable to increase from 30° to 45°. No significant effects of sweep on the stability were noted at Mach numbers of about 1.0 and 1.18. At all test Mach numbers, planform variation had no significant effect on the longitudinal stability at angles of attack from about 55° to the maximum of the test. (See fig. 17(a).)

The center-of-pressure location generally shifts rearward as the Mach number is increased from about 0.8 to 1.18 at angles of attack up to about 65°. (See

fig. 16.) Above this angle of attack, the effect of Mach number on the center-of-pressure location is small.

## Effect of Leading-Edge Shape

The primary effects on the aerodynamic characteristics of the 65° triangular-wing model due to changing the leading-edge shape from cylindrical to square were an increase in $C_{D,max}$ (fig. 15) and small positive pitching-moment increments throughout the angle-of-attack range (fig. 17(b)) without significantly affecting the center-of-pressure location (fig. 16). Small increases in the lift-curve slope at zero angle of attack and in the values of $C_{L,max}$ were also noted.

## Effects of Wing Lower Surface Contour

Ellipse model.- Comparison of the basic data of figures 6 and 7 shows that contouring the wing lower surface of the ellipse model to form the ellipse (convex) model caused a reduction in lift coefficient through the complete angle-of-attack range. This reduction in lift coefficient is associated with the effective negative camber of the ellipse (convex) model. The largest reductions in lift coefficient occurred near $C_{L,max}$; the magnitude of these losses can be seen in figure 15. The lift-curve slope of the ellipse (convex) model at zero angle of attack is slightly lower than that of the ellipse model. (See fig. 14.) The lift-curve slope of the ellipse (convex) model at 90° angle of attack is less negative than that of the ellipse model. (See fig. 15.)

The drag data of figure 14 indicate that contouring the bottom of the ellipse caused a large increase in minimum drag coefficient at Mach numbers of 1.01 and 1.18 but had a negligible effect on $C_{D,min}$ at a Mach number of 0.8. These increases in $C_{D,min}$ at Mach numbers of 1.01 and 1.18 are due largely to the increased pressure drag associated with the larger frontal area. The fact that there is a negligible effect on $C_{D,min}$ at a Mach number of 0.8 is attributed to the positive increment in base pressure of the ellipse (convex) model. (See fig. 3.) The values of maximum drag coefficient are considerably lower than those of the ellipse model at all test Mach numbers.

At Mach numbers of about 1.01 and 1.18, the ellipse (convex) model, because of its lower lift and higher drag, has lower values of $(L/D)_{max}$ than the ellipse model. The values of $(L/D)_{max}$ for both models were essentially the same at a Mach number of 0.8. (See fig. 14.)

At the three test Mach numbers, contouring the lower surface of the ellipse model caused positive increments in pitching moment with only small changes in the stability of the configuration. (See fig. 17(c).) These positive increments of pitching moment are associated with a forward movement of the center of pressure, particularly at angles of attack below about 35°. (See fig. 16.) This forward movement of the center of pressure results from the combined effect of the positive pressures (caused by the higher local slopes) acting on the

forward part of the wing lower surface and the reduction in pressure (caused by the decrease in local slope) acting on the aft part of the wing lower surface.

Trihedron.- Contouring the wing lower surface of the 75° model to form the trihedron model caused an increase in lift coefficient up to an angle of attack of about 20° for the three test Mach numbers (see figs. 11 and 13) without significantly affecting $C_{L_{\alpha,0^\circ}}$ (fig. 14). This increase in lift coefficient is associated with the increase in effective angle of attack of the trihedron model. Above an angle of attack of about 20°, the trihedron model has the lower lift and the reduction in the values of $C_{L,max}$ is shown in figure 15. The lift-curve slope at an angle of attack of 90° was less negative for the trihedron model than for the 75° model at all test Mach numbers. (See fig. 15.)

The drag data of figure 13 indicate that the minimum drag of the trihedron model was not obtained within the present angle-of-attack range. Therefore, figure 14 does not present values of $C_{D,min}$ for the trihedron model. A comparison of the drag data of figures 11 and 13, however, indicates that the minimum drag of the trihedron model would be substantially higher than that of the 75° model. The trihedron model has higher values of drag coefficient than the 75° model up to an angle of attack of about 50° at Mach numbers of about 1.01 and 1.18 and up to an angle of attack of 40° at a Mach number of about 0.8. Above these angles of attack, the drag of the trihedron model was lower than that of the 75° model. (See figs. 11 and 13.) This lower drag of the trihedron model at the large values of angle of attack was probably associated with the pressure relief afforded by the vee-shape of the wing lower surfaces. As would be expected, the maximum drag of the trihedron model occurred at an angle of attack of about 75°. At this angle of attack, the ridgeline of the trihedron model was perpendicular to the free-stream direction and the wing lower surfaces were at the largest angle to the free-stream direction. Maximum drag for the 75° model occurred at an angle of attack of 90°.

As shown in figure 14, the values of $(L/D)_{max}$ for the trihedron model vary between about 1.8 and 1.3 through the Mach number range. These values of $(L/D)_{max}$ are the lowest of any of the configurations tested and are about 50 percent lower than those of the 75° model. The low values of maximum lift-drag ratio are due primarily to the high drag of the trihedron model.

For all angles of attack of the present test, contouring the wing of the 75° model to form the trihedron model generally caused large negative increments in pitching-moment coefficient. (See fig. 17(d).) At low angles of attack ($\alpha < 15^\circ$), small increases in the longitudinal stability are noted for the trihedron model. The trihedron model appears to be the most stable configuration investigated. The center of pressure for this configuration is always behind the present moment reference location except at angles of attack between 15° and 52° at a Mach number of 0.8. (See fig. 16.)

## SUMMARY OF RESULTS

An investigation has been conducted in the Langley transonic blowdown tunnel to determine the effects of wing planform and other geometric parameters on the static longitudinal aerodynamic characteristics of winged vehicles suitable for reentry. Wing leading-edge radius and wing lower surface contour were also varied for several of the configurations during the investigation. The tests were made at Mach numbers of about 0.8, 1.01, and 1.18 for angles of attack that generally varied from -4° to 91°.

The results of the investigation indicate the following:

1. At a given test Mach number, planform variation for the basic models had a considerable effect on lift-curve slope at an angle of attack of 0° but had essentially no effect on maximum lift coefficient, lift-curve slope at an angle of attack of 90°, or maximum drag coefficient.

2. The values of maximum lift-drag ratio for the circle model varied between 2.5 and 3.0 while those of the other basic planforms generally varied between 3 and 4.

3. The basic planforms were longitudinally unstable below the angle of attack at which maximum lift was obtained and longitudinally stable above this angle of attack with the moment reference point located at the centroid of planform area of each planform.

4. Changing the leading edge of the 65° triangular model from cylindrical to square caused higher maximum drag and generally small positive increments in pitching moment through the test angle-of-attack range.

5. Contouring the wing lower surface of the ellipse model to form the ellipse (convex) model caused positive increments in pitching moment, decreases in lift coefficient and maximum drag coefficient, and small changes in stability.

6. Contouring the wing lower surface of the 75° model to form the trihedron model caused large negative increments in pitching-moment coefficient, an increase in lift coefficient below and a decrease in lift coefficient above an angle of attack of 20°, and an increase in drag coefficient below an angle of attack of about 50°. The trihedron model had the lowest maximum lift-drag ratio of the configurations tested.

Langley Research Center,
National Aeronautics and Space Administration,
Langley Station, Hampton, Va., February 18, 1963.

## REFERENCES


1. Staff of Langley Flight Research Division (Donald C. Cheatham, Compiler): A Concept of a Manned Satellite Reentry Which Is Completed With a Glide Landing. NASA TM X-226, 1959.

2. Foster, Gerald V.: Longitudinal Aerodynamic Characteristics at a Mach Number of 1.97 of a Series of Related Winged Reentry Configurations for Angles of Attack From 0° to 90°. NASA TM X-461, 1961.

3. Smith, Fred M., and Nichols, Frank H., Jr.: A Wind-Tunnel Investigation of the Aerodynamic Characteristics of a Generalized Series of Winged Reentry Configurations at Angles of Attack to 180° at Mach Numbers of 2.38, 2.99, and 4.00. NASA TM X-512, 1961.

4. Putnam, Lawrence E., and Brooks, Cuyler W., Jr.: Static Longitudinal Aerodynamic Characteristics at a Mach Number of 10.03 of Low-Aspect-Ratio Wing-Body Configurations Suitable for Reentry. NASA TM X-733, 1962.

5. Braslow, Albert L., and Knox, Eugene C.: Simplified Method for Determination of Critical Height of Distributed Roughness Particles for Boundary-Layer Transition at Mach Numbers From 0 to 5. NACA TN 4363, 1958.

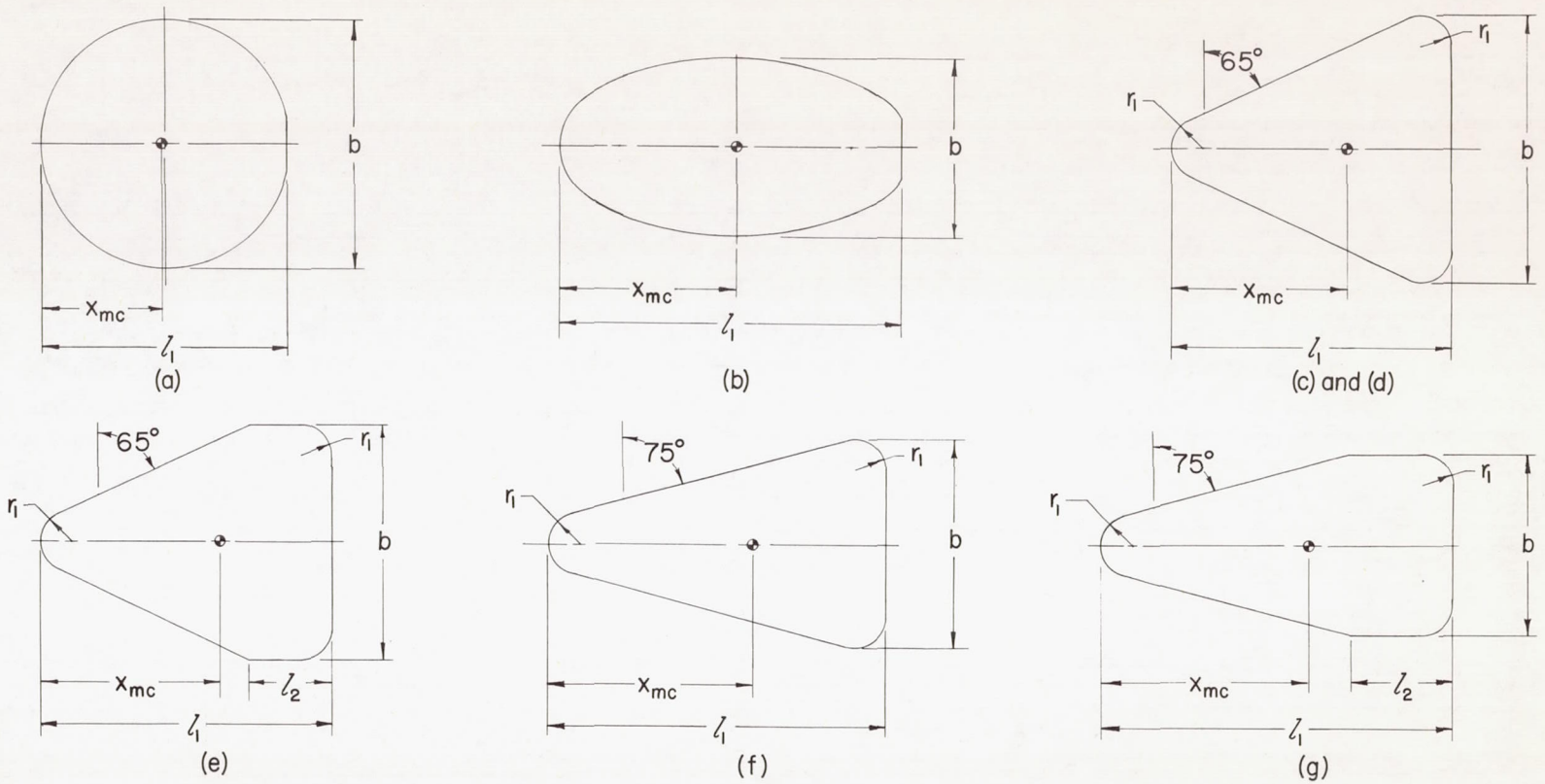


| | Small models | | | | | Large models | | | | |
|---|---|---|---|---|---|---|---|---|---|---|
| | $l_1$ | $l_2$ | b | $r_1$ | $x_{mc}$ | $l_1$ | $l_2$ | b | $r_1$ | $x_{mc}$ |
| (a) Circle | 2.961 | | 3.000 | | 1.496 | 4.356 | | 4.414 | | 2.201 |
| (b) Ellipse | 4.130 | | 2.121 | | 2.074 | 6.076 | | 3.121 | | 3.051 |
| (c) 65° | 3.381 | | 3.204 | 0.375 | 2.102 | 4.975 | | 4.714 | 0.552 | 3.094 |
| (d) 65° (Square leading edge) | 3.381 | | 3.204 | .375 | 2.102 | 4.975 | | 4.714 | .552 | 3.094 |
| (e) 65° (Clipped) | 3.507 | 0.996 | 2.820 | .375 | 2.141 | 5.137 | 1.461 | 4.133 | .552 | 3.128 |
| (f) 75° | 4.063 | | 2.524 | .375 | 2.462 | 5.977 | | 3.714 | .552 | 3.622 |
| (g) 75° (Clipped) | 4.215 | 1.259 | 2.160 | .375 | 2.492 | 6.204 | 1.861 | 3.175 | .552 | 3.670 |

(a) Basic planform configurations.

Figure 1.- Model drawings and dimensions. All dimensions are in inches.

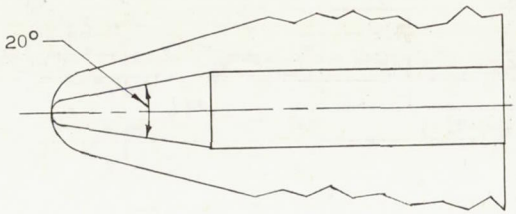


| Small models | $l_1$ | $l_4$ | $h_1$ | t | $r_2$ | $r_3$ |
|---|---|---|---|---|---|---|
| (a) Circle | 2.961 | 1.545 | 0.555 | 0.125 | 0.108 | 0.340 |
| (b) Ellipse | 4.130 | 2.714 | .555 | .125 | .108 | .340 |
| (c) 65° | 3.381 | 1.965 | .555 | .125 | .108 | .340 |
| (d) 65° (Square leading edge) | 3.381 | 1.965 | .555 | .125 | .108 | .340 |
| (e) 65° (Clipped) | 3.507 | 2.091 | .555 | .125 | .108 | .340 |
| (f) 75° | 4.063 | 2.647 | .555 | .125 | .108 | .340 |
| (g) 75° (Clipped) | 4.215 | 2.799 | .555 | .125 | .108 | .340 |

| Large models | $l_1$ | $l_4$ | $h_1$ | t | $r_2$ | $r_3$ |
|---|---|---|---|---|---|---|
| (a) Circle | 4.356 | 2.274 | 0.817 | 0.183 | 0.158 | 0.500 |
| (b) Ellipse | 6.076 | 3.994 | .817 | .183 | .158 | .500 |
| (c) 65° | 4.975 | 2.893 | .817 | .183 | .158 | .500 |
| (d) 65° (Square leading edge) | 4.975 | 2.893 | .817 | .183 | .158 | .500 |
| (e) 65° (Clipped) | 5.137 | 3.055 | .817 | .183 | .158 | .500 |
| (f) 75° | 5.977 | 3.895 | .817 | .183 | .158 | .500 |
| (g) 75° (Clipped) | 6.204 | 4.122 | .817 | .183 | .158 | .500 |

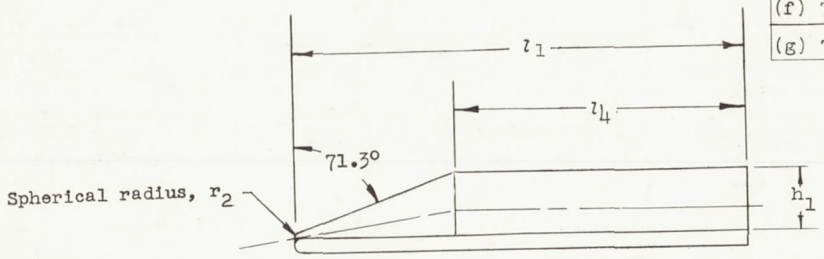


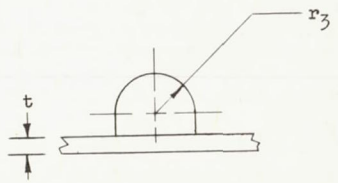


(b) Body and nose drawings and dimensions.

Figure 1.- Continued.

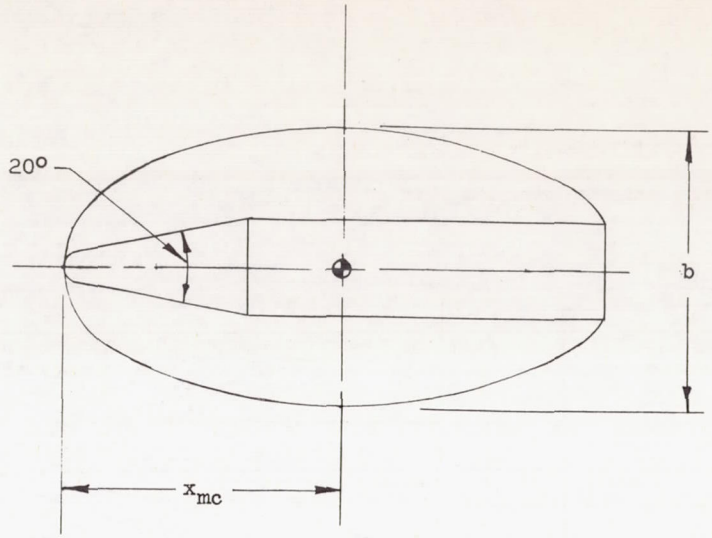


| | Small models | Large models |
|---|---|---|
| $l_1$ | 4.130 | 6.076 |
| $l_4$ | 2.714 | 3.994 |
| b | 2.121 | 3.121 |
| $h_1$ | 0.555 | 0.817 |
| $r_2$ | .108 | .158 |
| $r_3$ | .340 | .500 |
| $r_4$ | .062 | .092 |
| $x_{mc}$ | 2.074 | 3.051 |

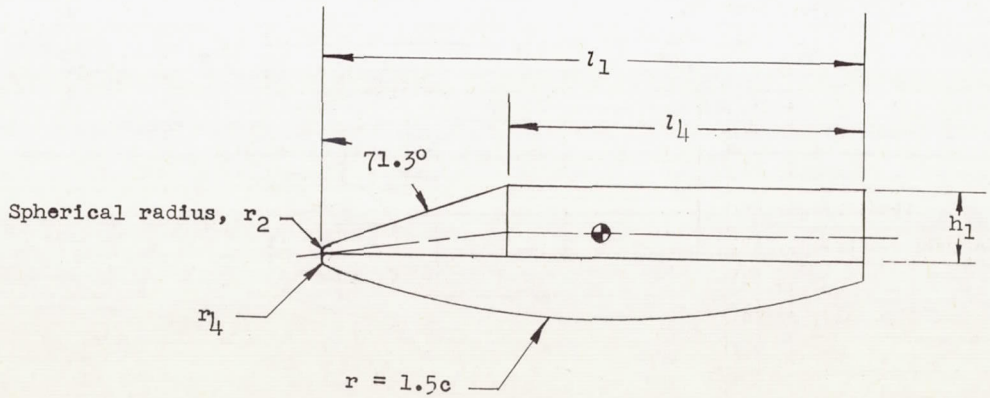


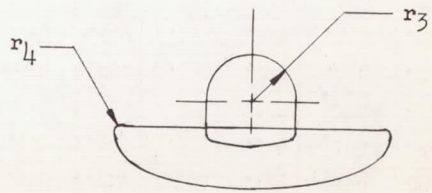


(c) Ellipse (convex) model.

Figure 1.- Continued.

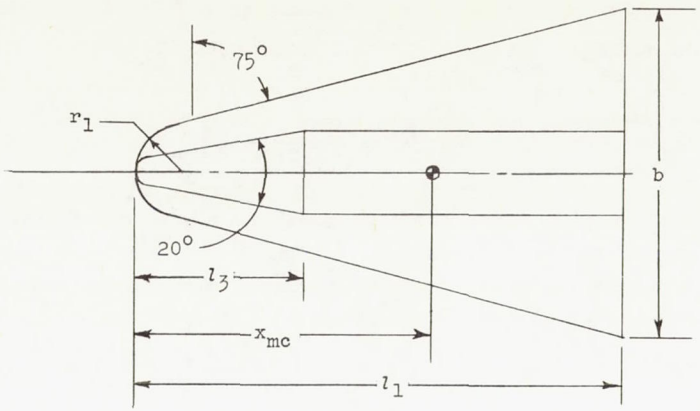


| | Small models | Large models |
|---|---|---|
| $l_1$ | 4.063 | 5.977 |
| $l_3$ | 1.416 | 2.082 |
| $r_1$ | .375 | .552 |
| $r_2$ | .108 | .158 |
| $r_3$ | .340 | .500 |
| $x_{mc}$ | 2.488 | 3.660 |
| $h_1$ | .555 | .817 |
| $h_2$ | 1.865 | 2.743 |
| b | 2.752 | 4.050 |

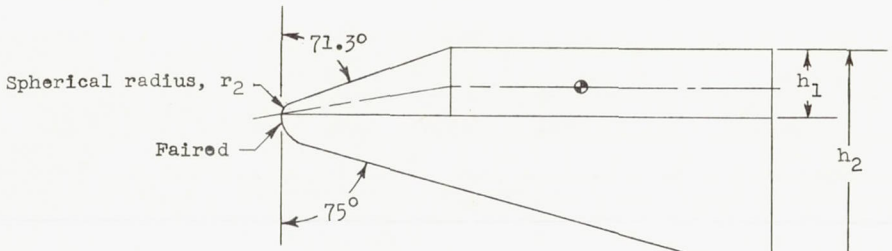


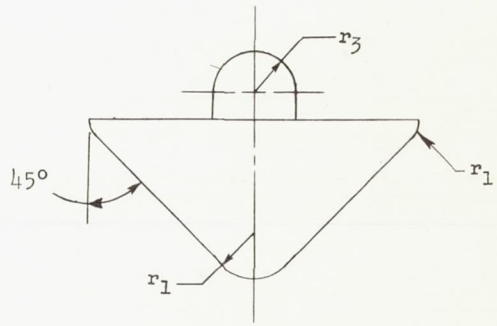


(d) Trihedron model.

Figure 1.- Concluded.

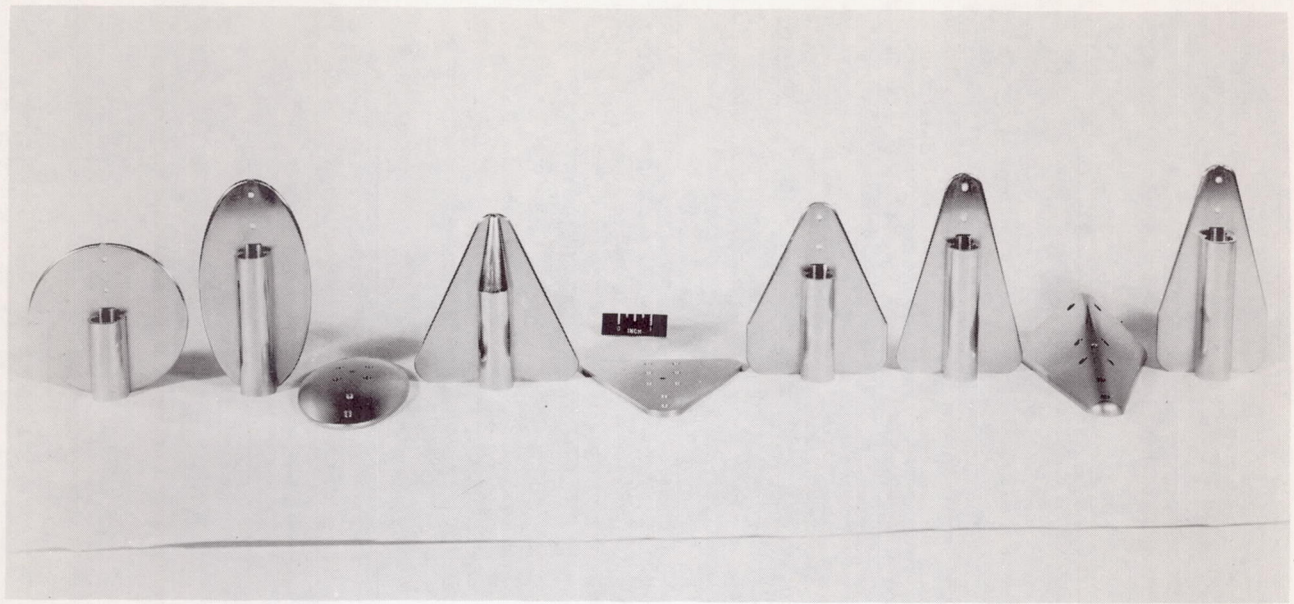

(a) Large models ($\alpha < 46°$). L-59-7617

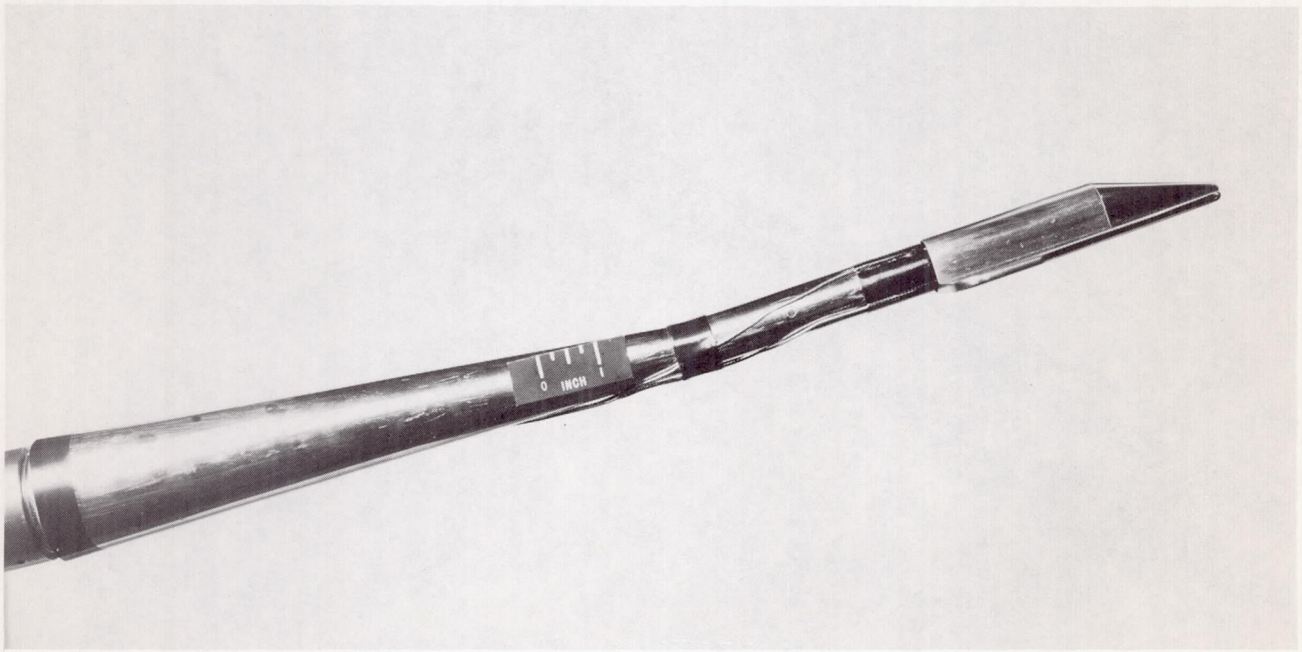


(b) Model mounting arrangement at low angles of attack. L-60-7845

Figure 2.- Photographs of model configurations.

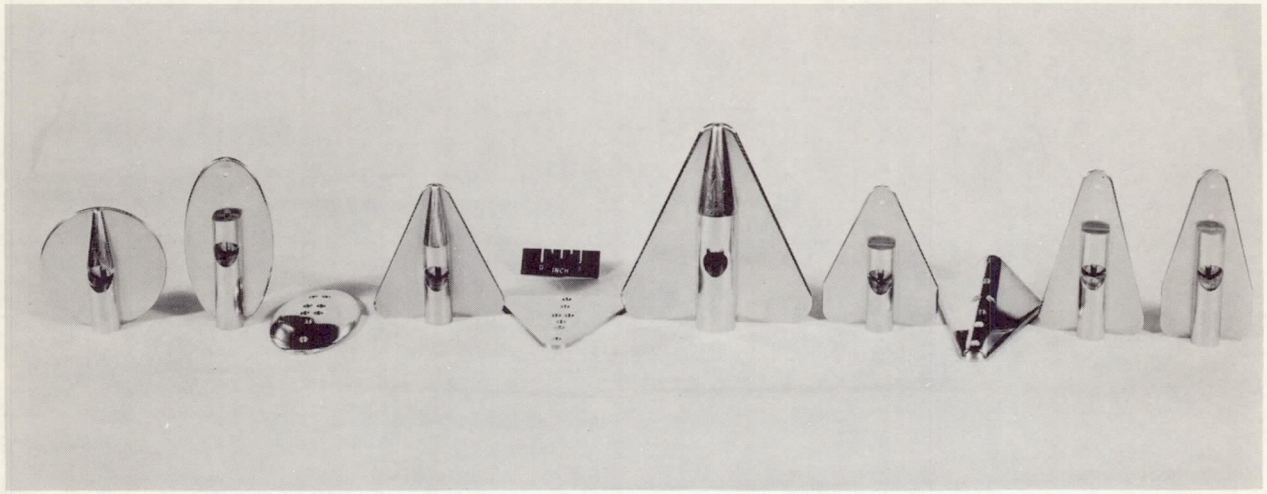

(c) Small models ($\alpha > 50°$). L-59-7619

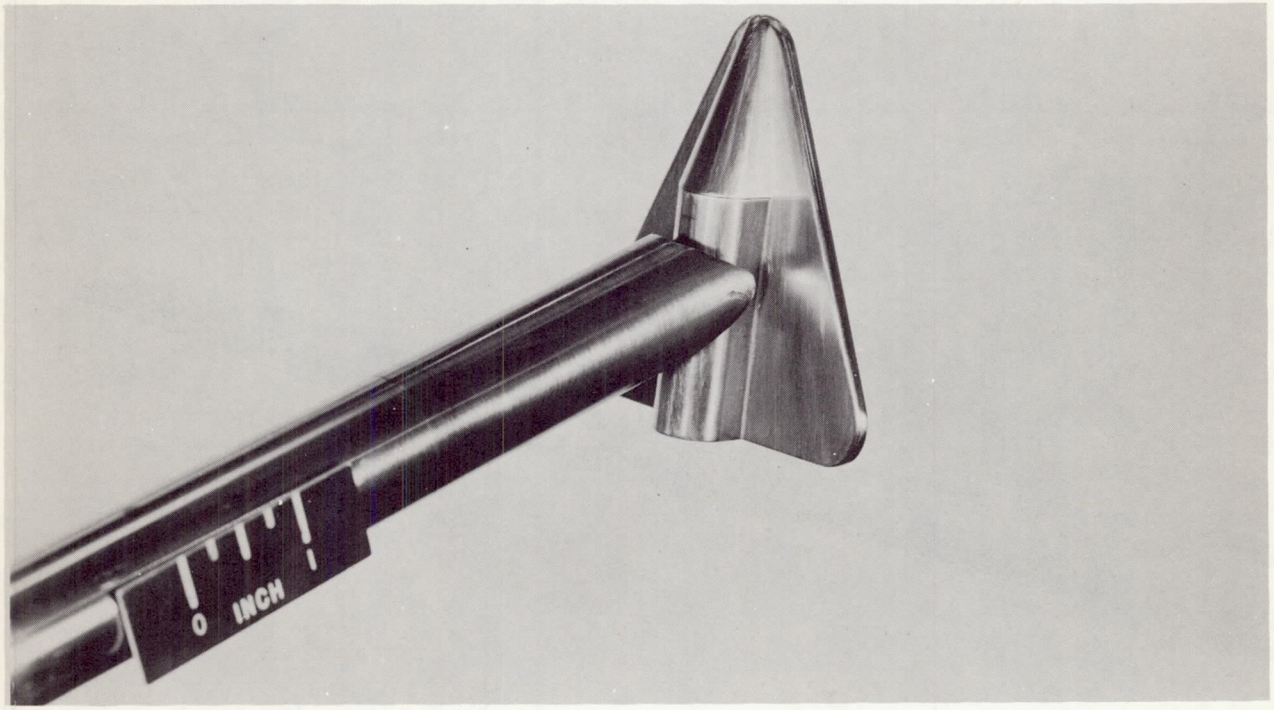


(d) Model mounting arrangement at high angles of attack. L-59-7620

Figure 2.- Concluded.

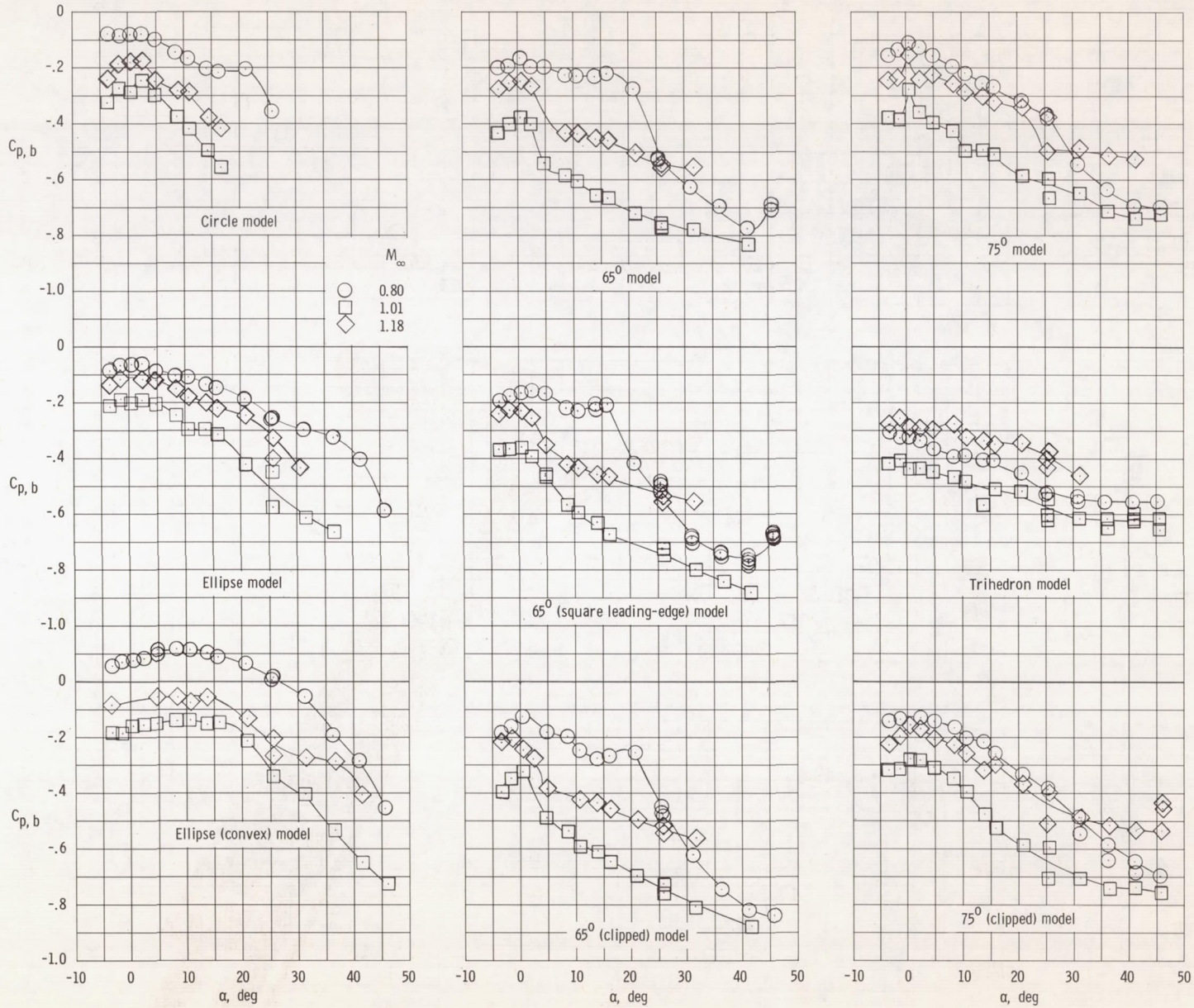


Figure 3.- Effect of Mach number on the base pressures of the various configurations.

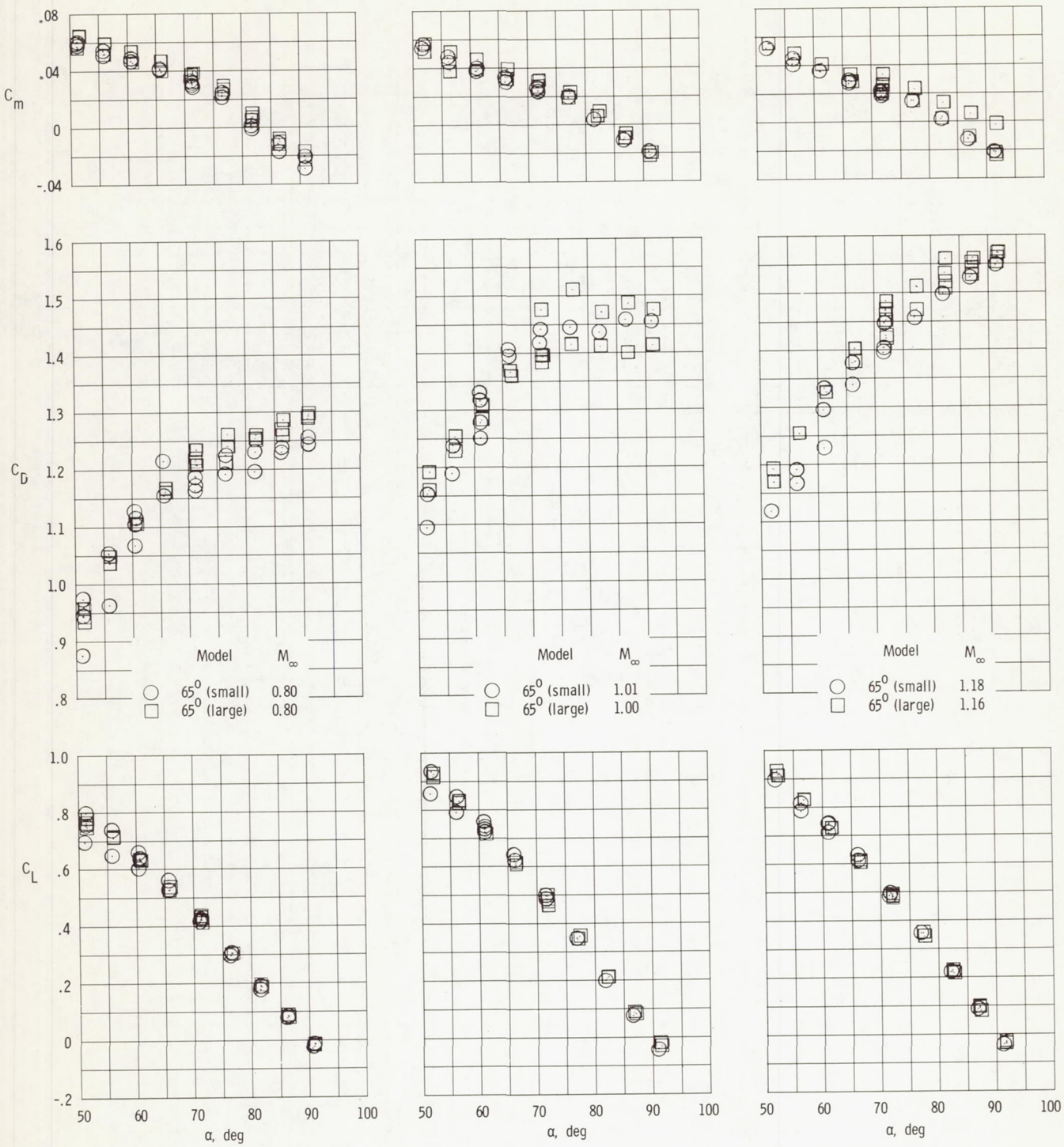


Figure 4.- Comparison of the longitudinal aerodynamic characteristics for two size models of the 65° configuration.

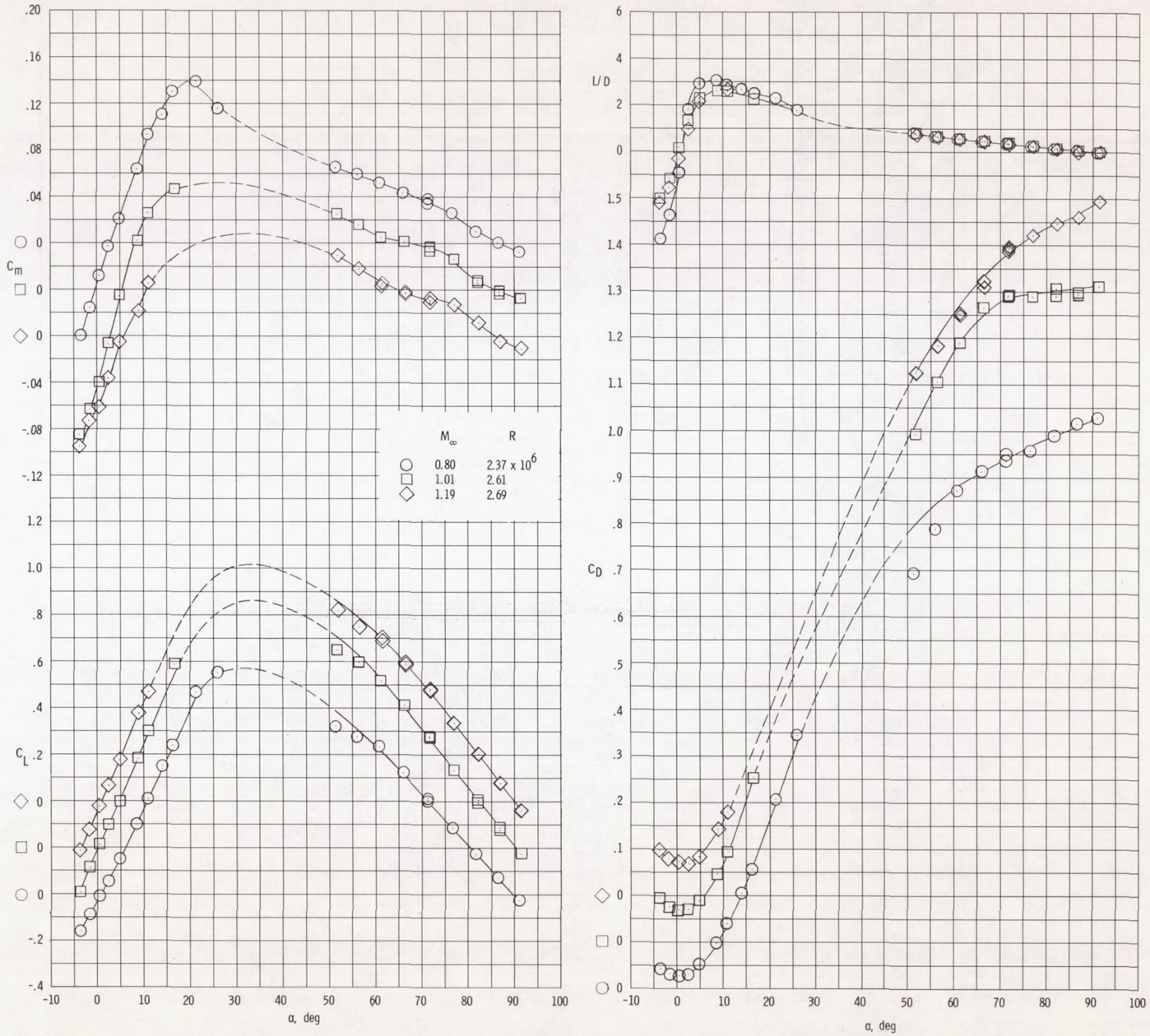


Figure 5.- Longitudinal aerodynamic characteristics of the circle model.

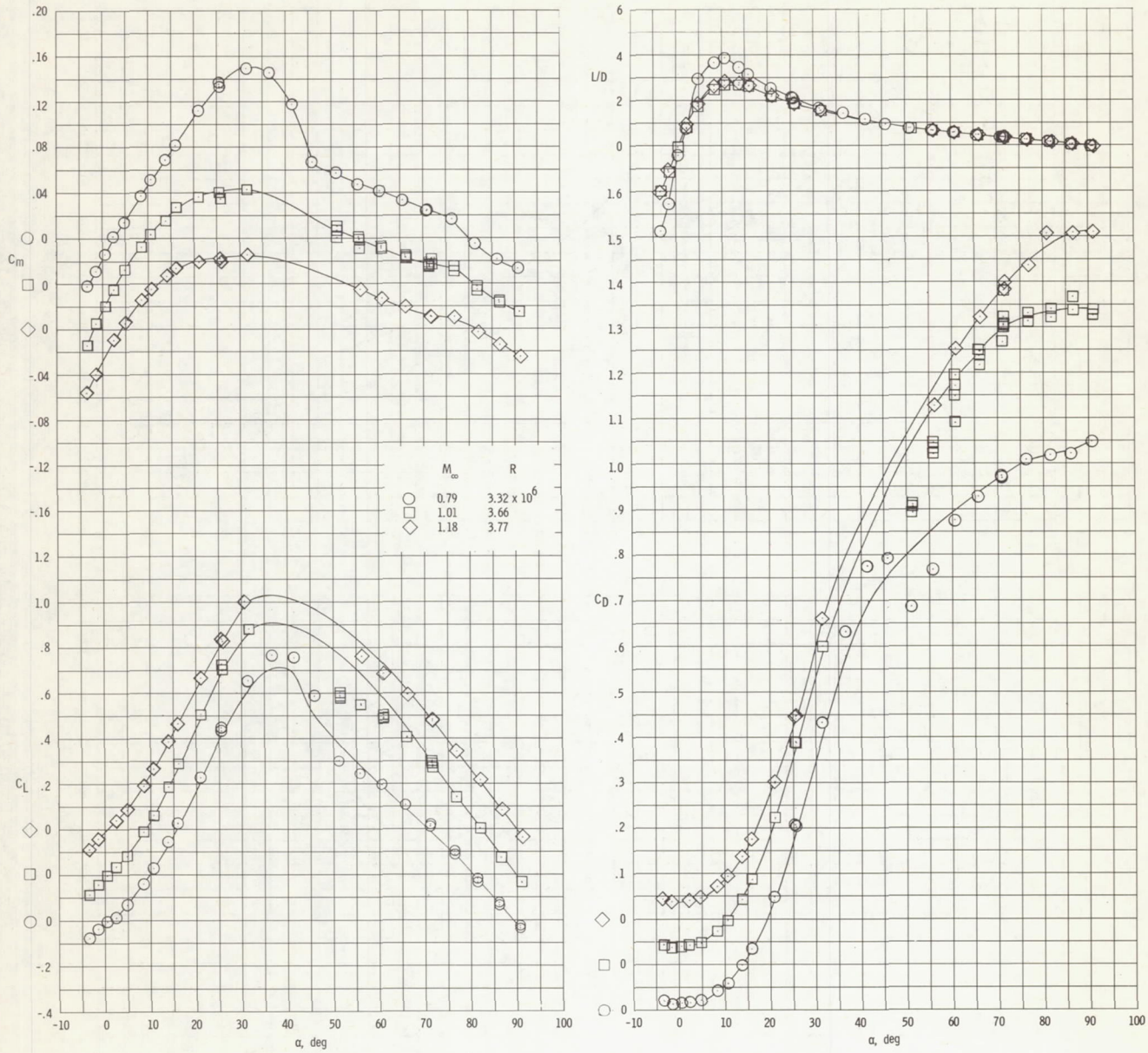


Figure 6.- Longitudinal aerodynamic characteristics of the ellipse model.

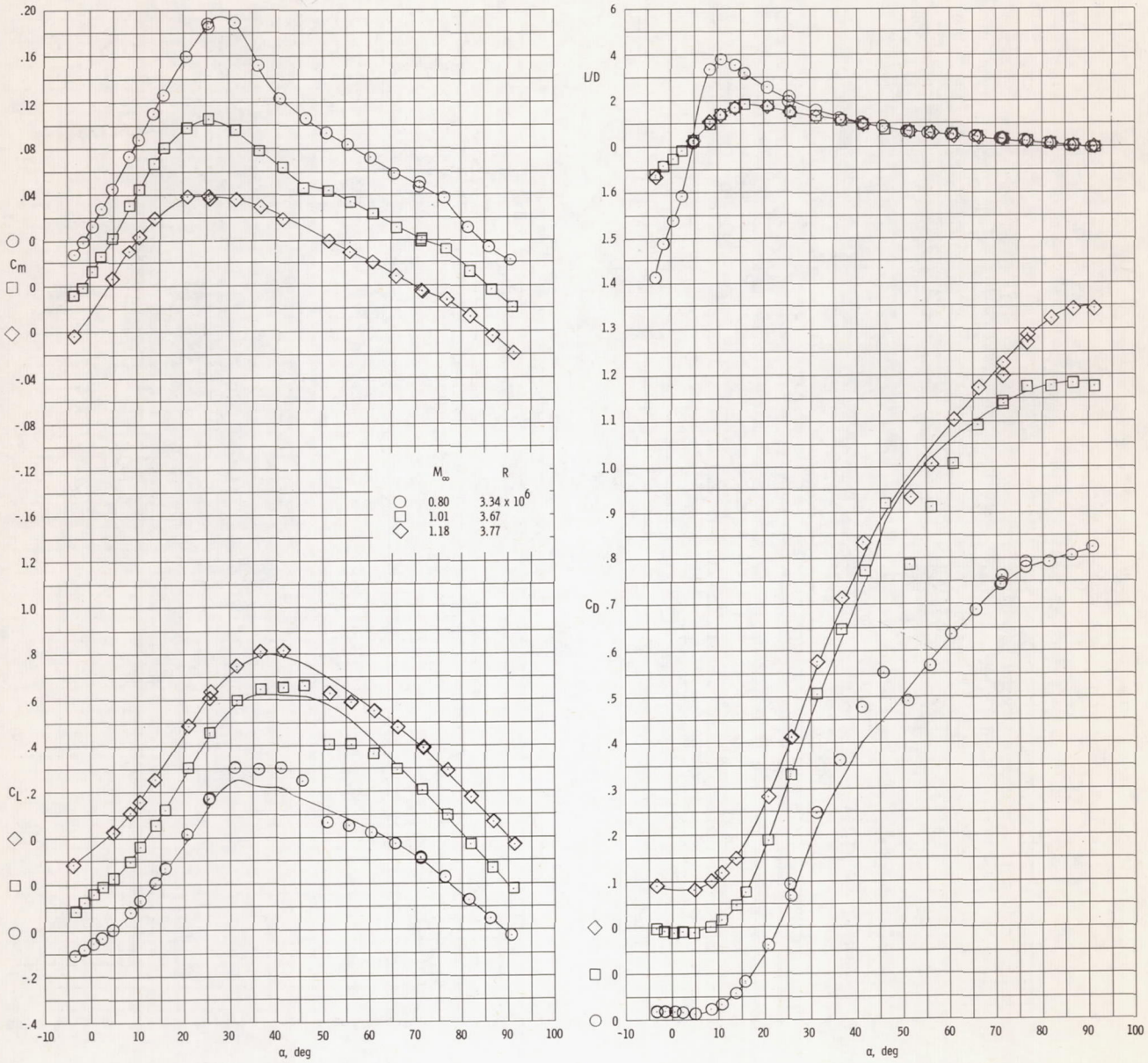


Figure 7.- Longitudinal aerodynamic characteristics of the ellipse (convex) model.

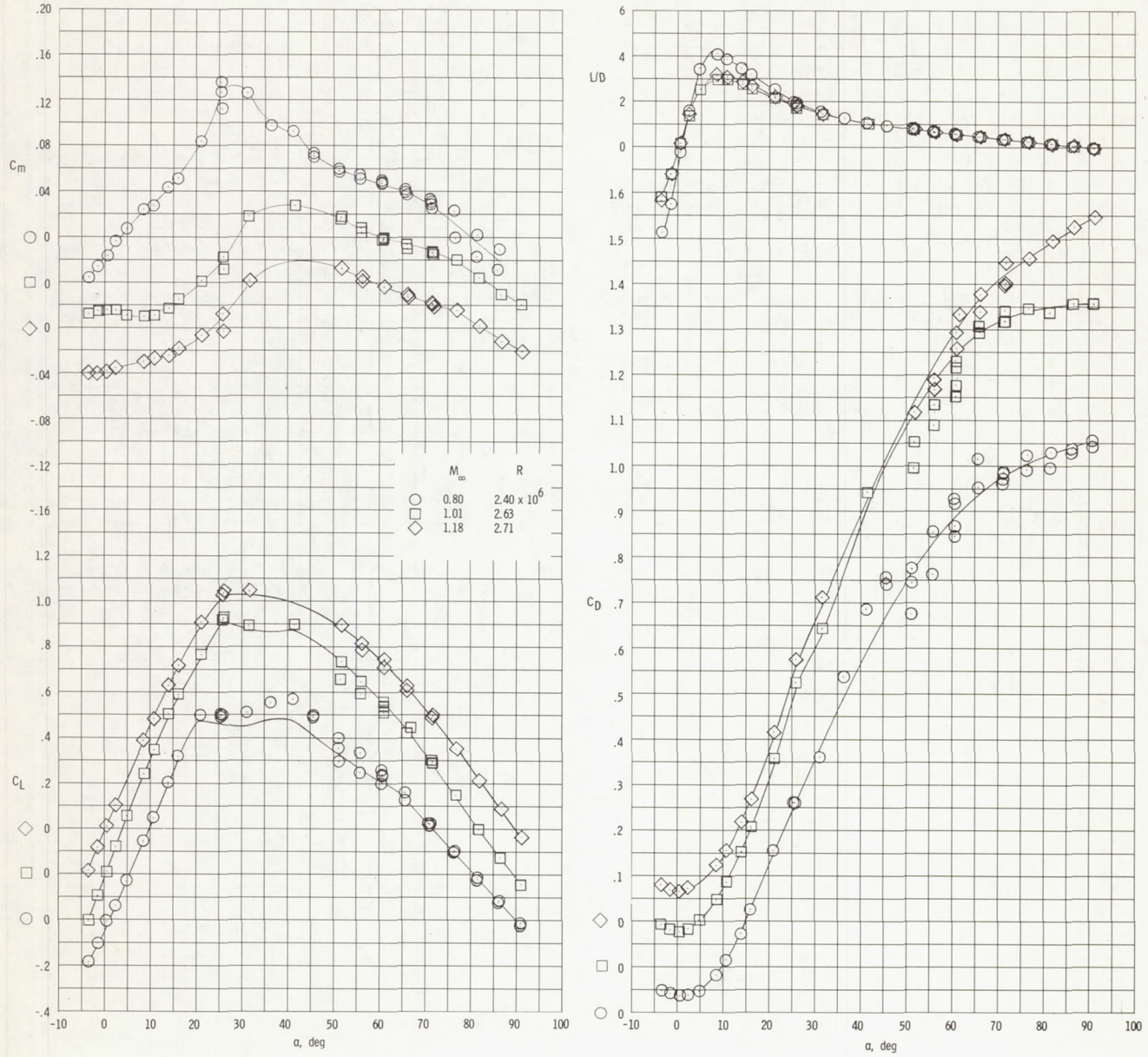


Figure 8.- Longitudinal aerodynamic characteristics of the 65° model.

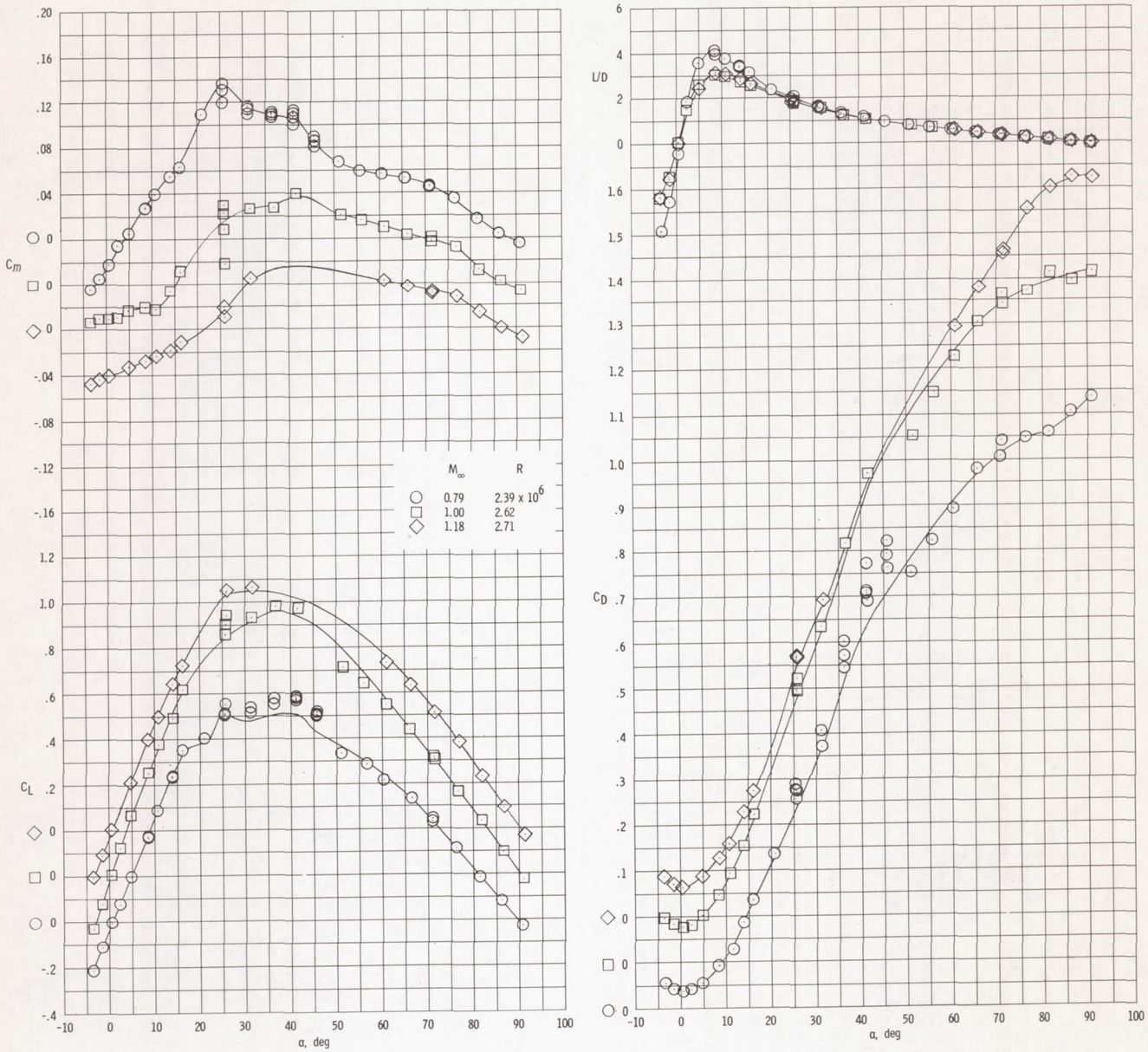


Figure 9.- Longitudinal aerodynamic characteristics of the 65° (square leading-edge) model.

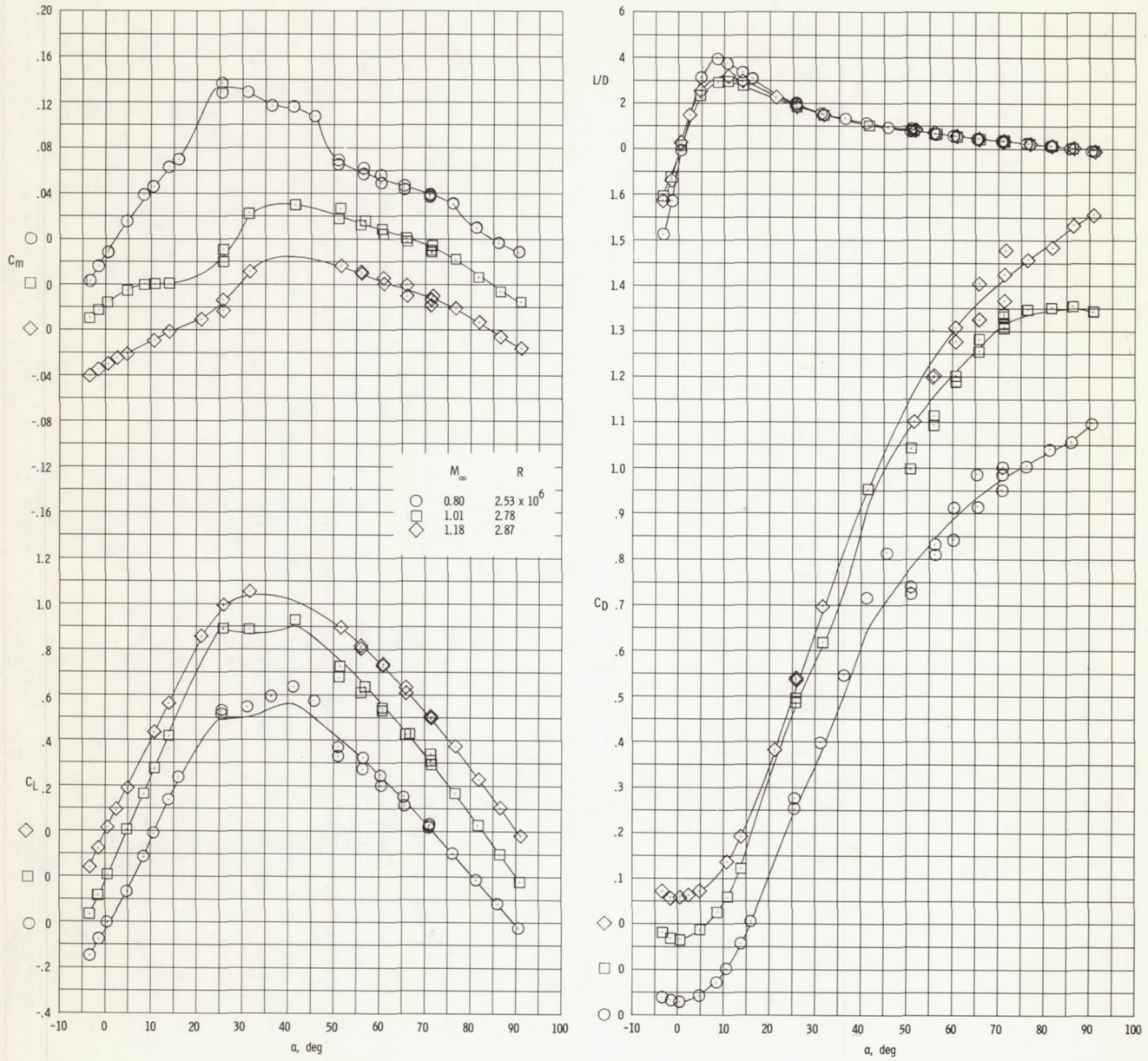


Figure 10.- Longitudinal aerodynamic characteristics of the 65° (clipped) model.

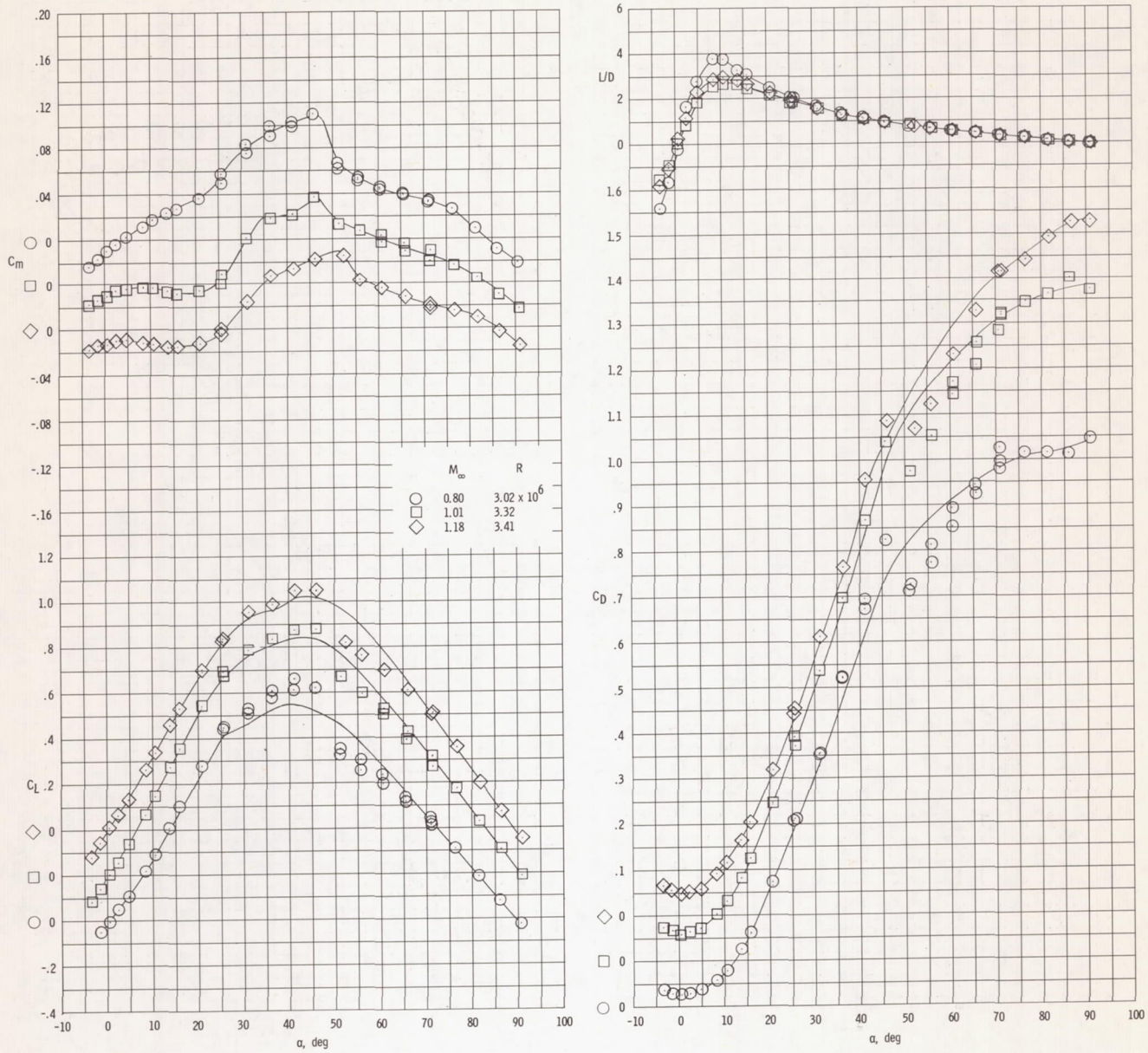


Figure 11.- Longitudinal aerodynamic characteristics of the 75° model.

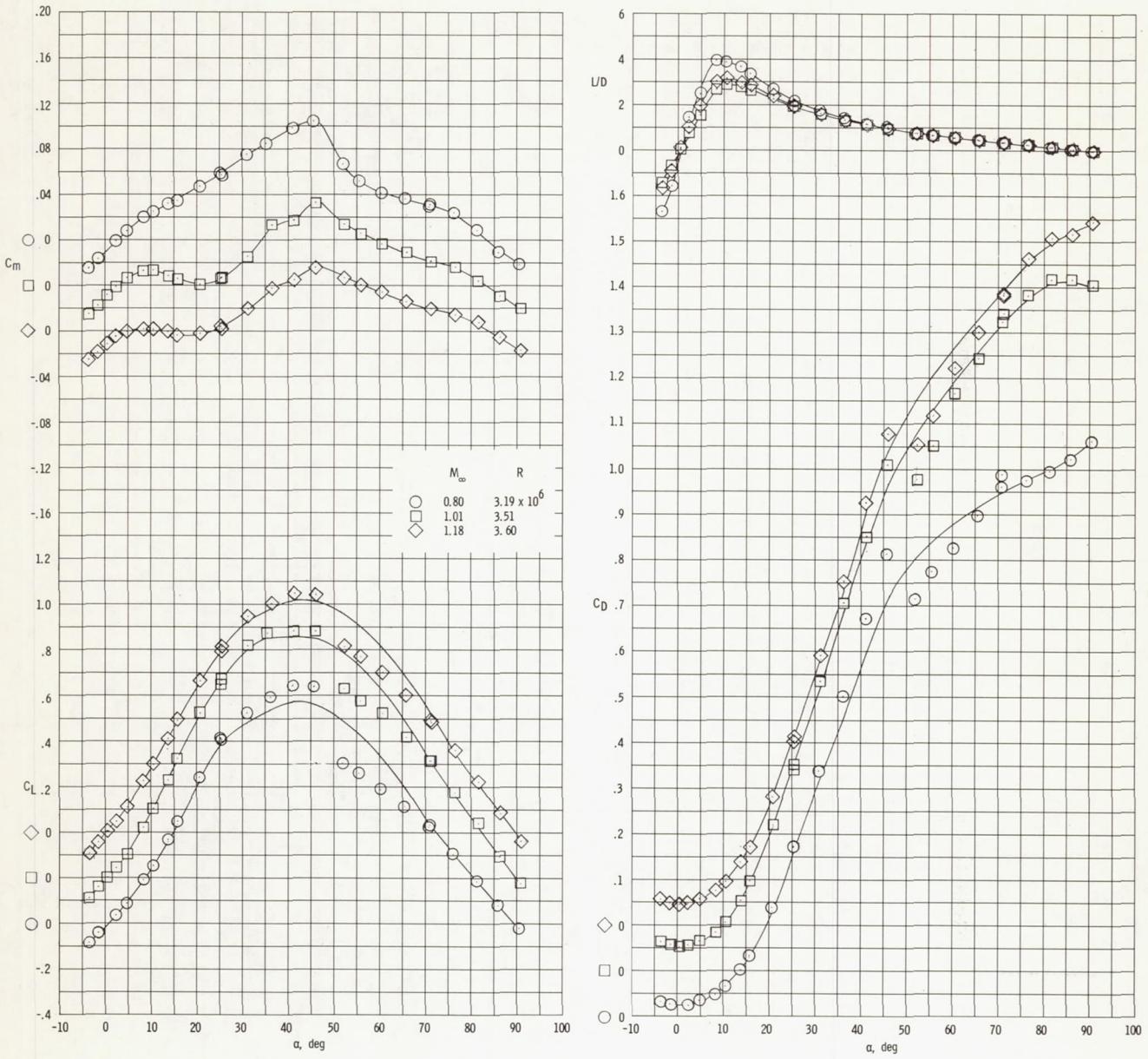


Figure 12.- Longitudinal aerodynamic characteristics of the 75° (clipped) model.

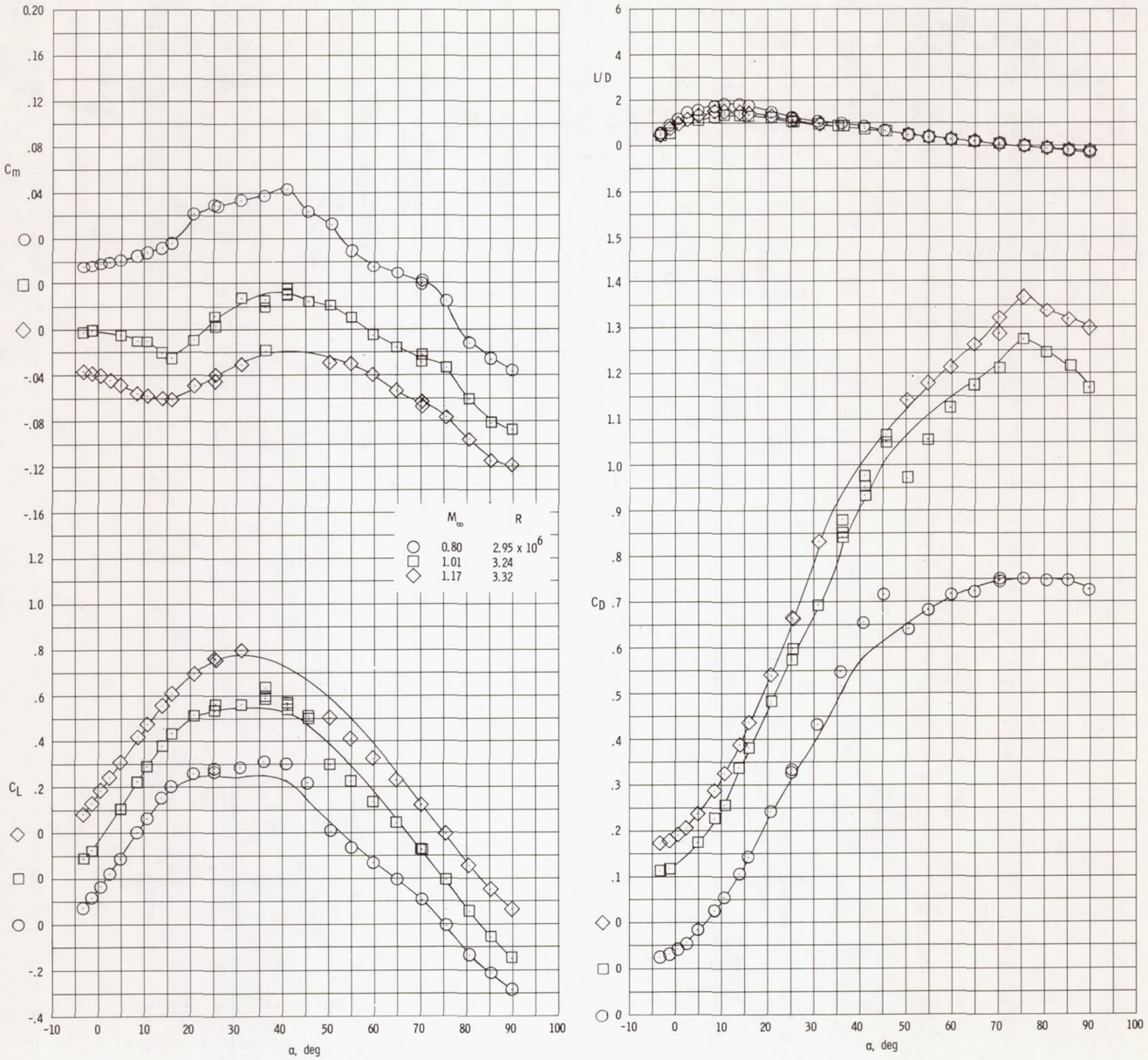


Figure 13.- Longitudinal aerodynamic characteristics of the trihedron model.

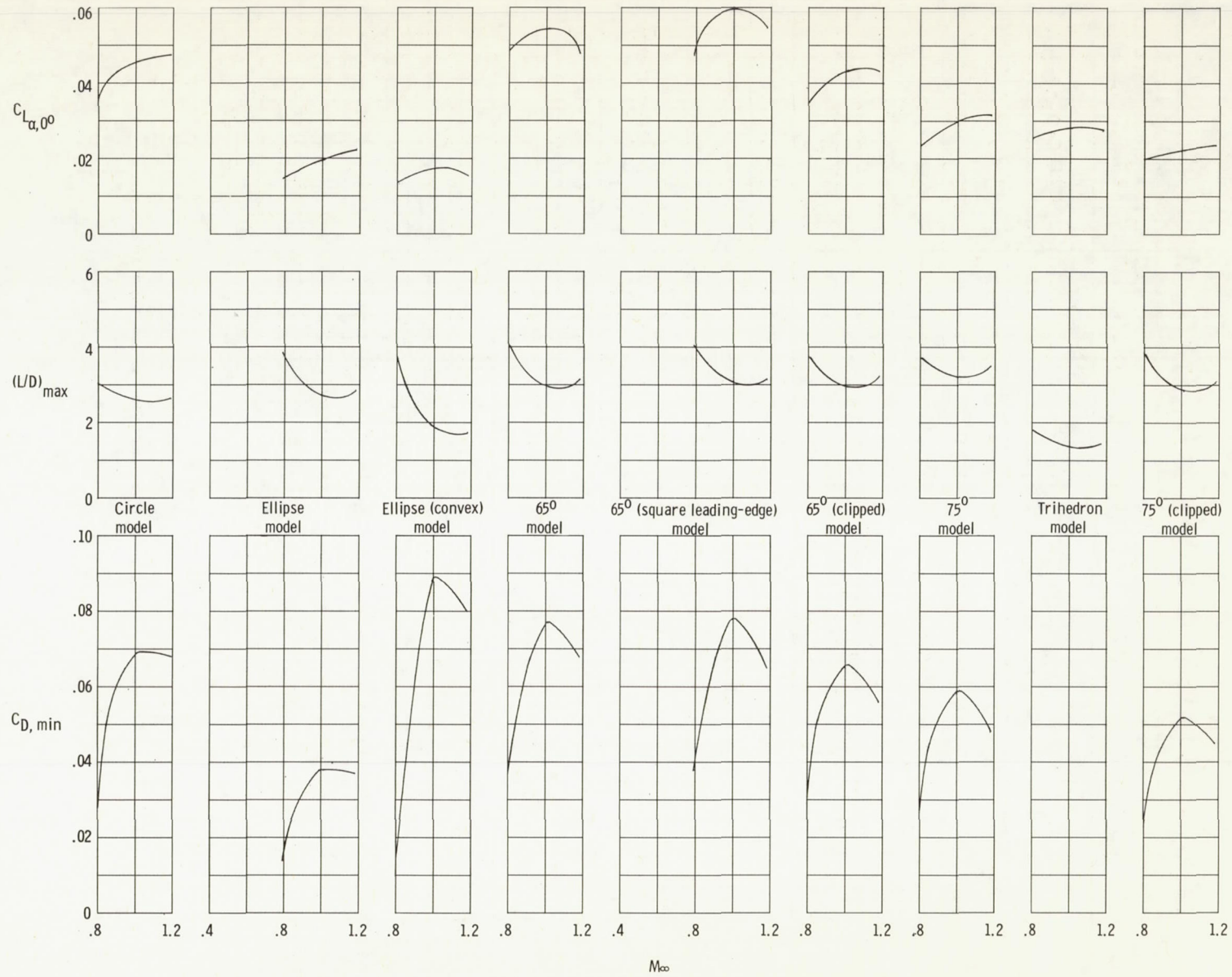


Figure 14.- Effect of Mach number on $C_{L_{\alpha,0^o}}$, $(L/D)_{max}$, and $C_{D,min}$ for each configuration.

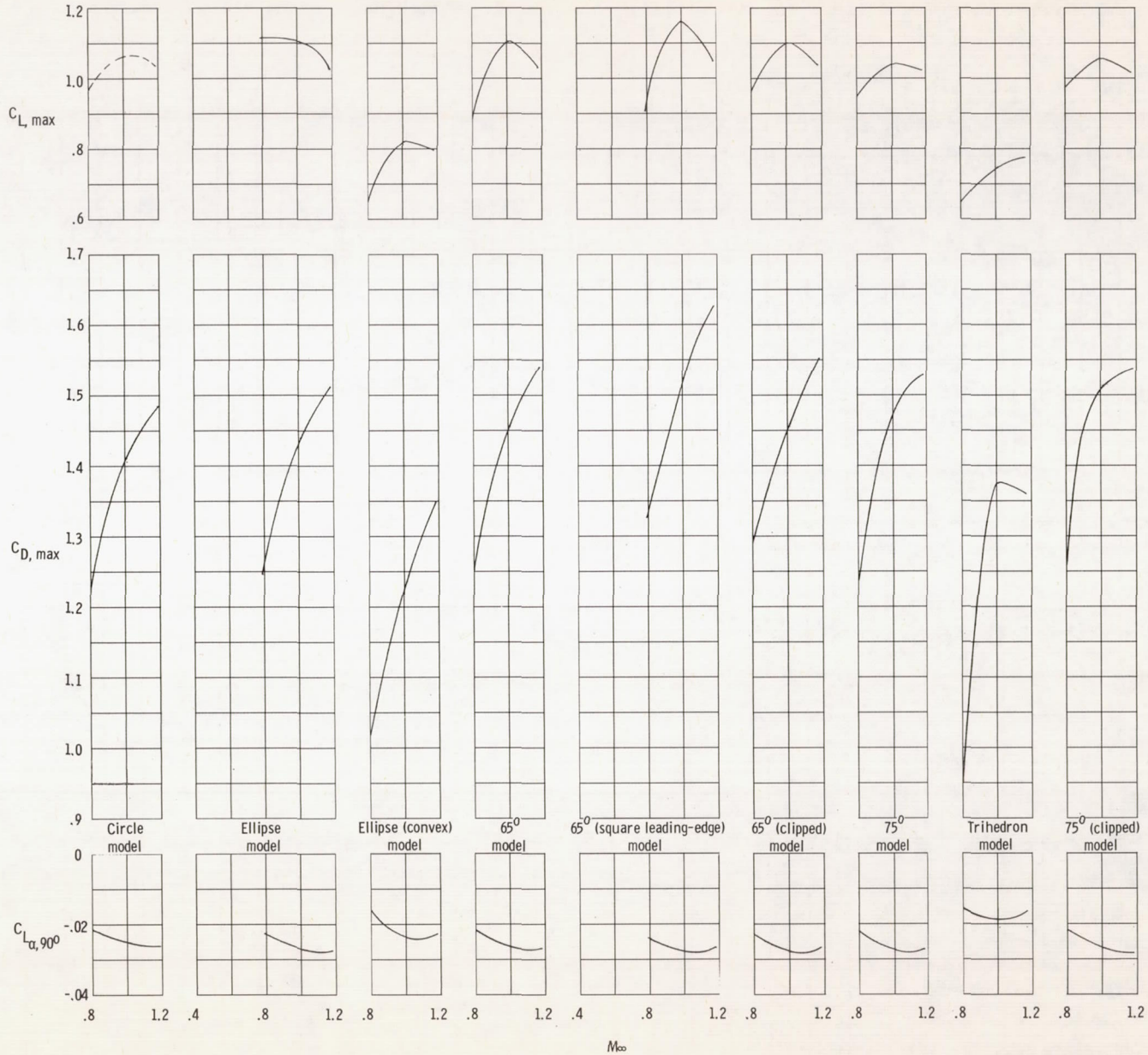


Figure 15.- Effect of Mach number on $C_{L,max}$, $C_{D,max}$, and $C_{L_\alpha,90^\circ}$ for each configuration.

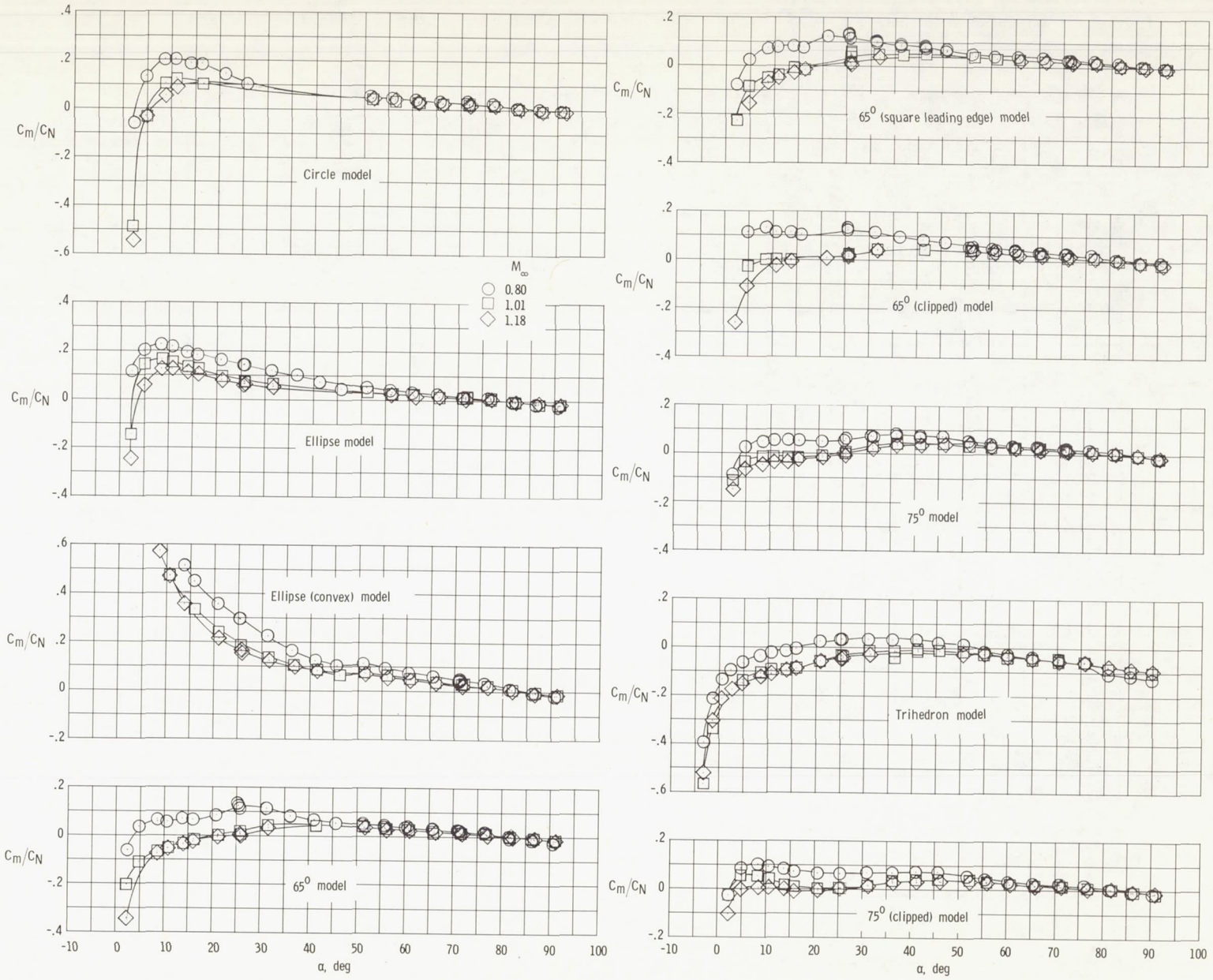


Figure 16.- Effect of Mach number on variation of center of pressure with angle of attack for each configuration.

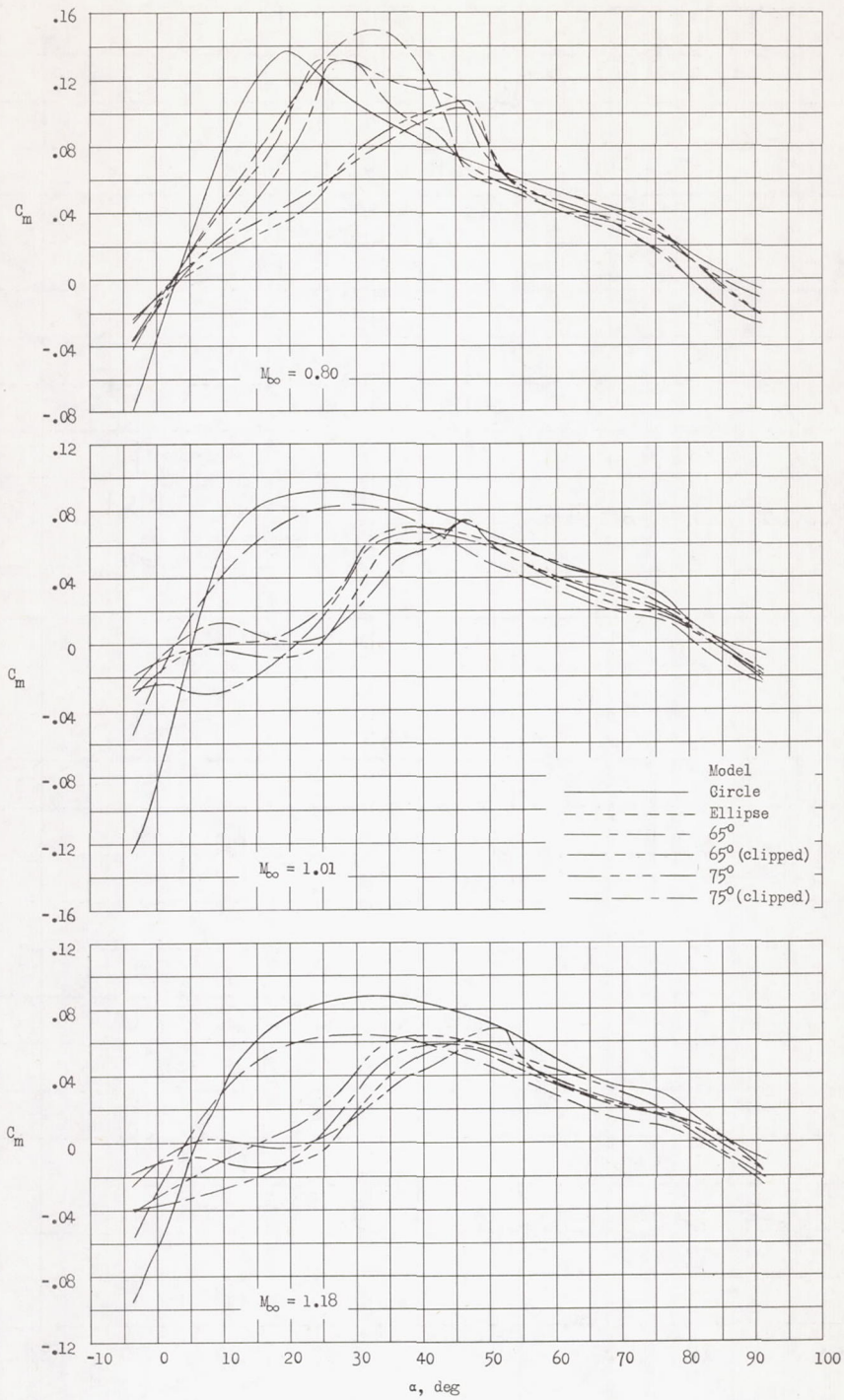


(a) Basic planform variation.

Figure 17.- Effect of planform, leading-edge shape, and lower surface contour on the variation of pitching-moment coefficient with angle of attack at Mach numbers of 0.80, 1.01, and 1.18.

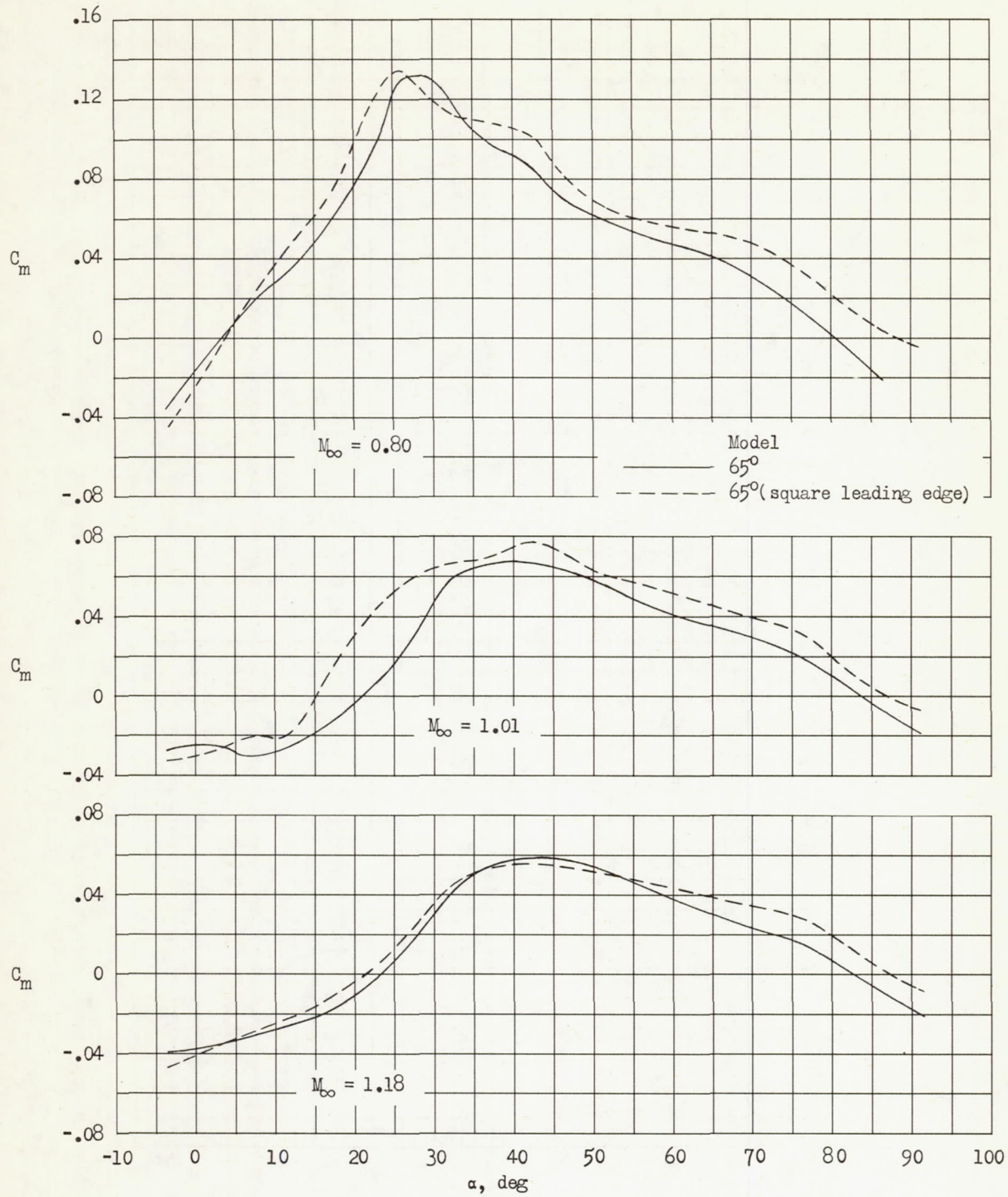


(b) Leading-edge shape.

Figure 17.- Continued.

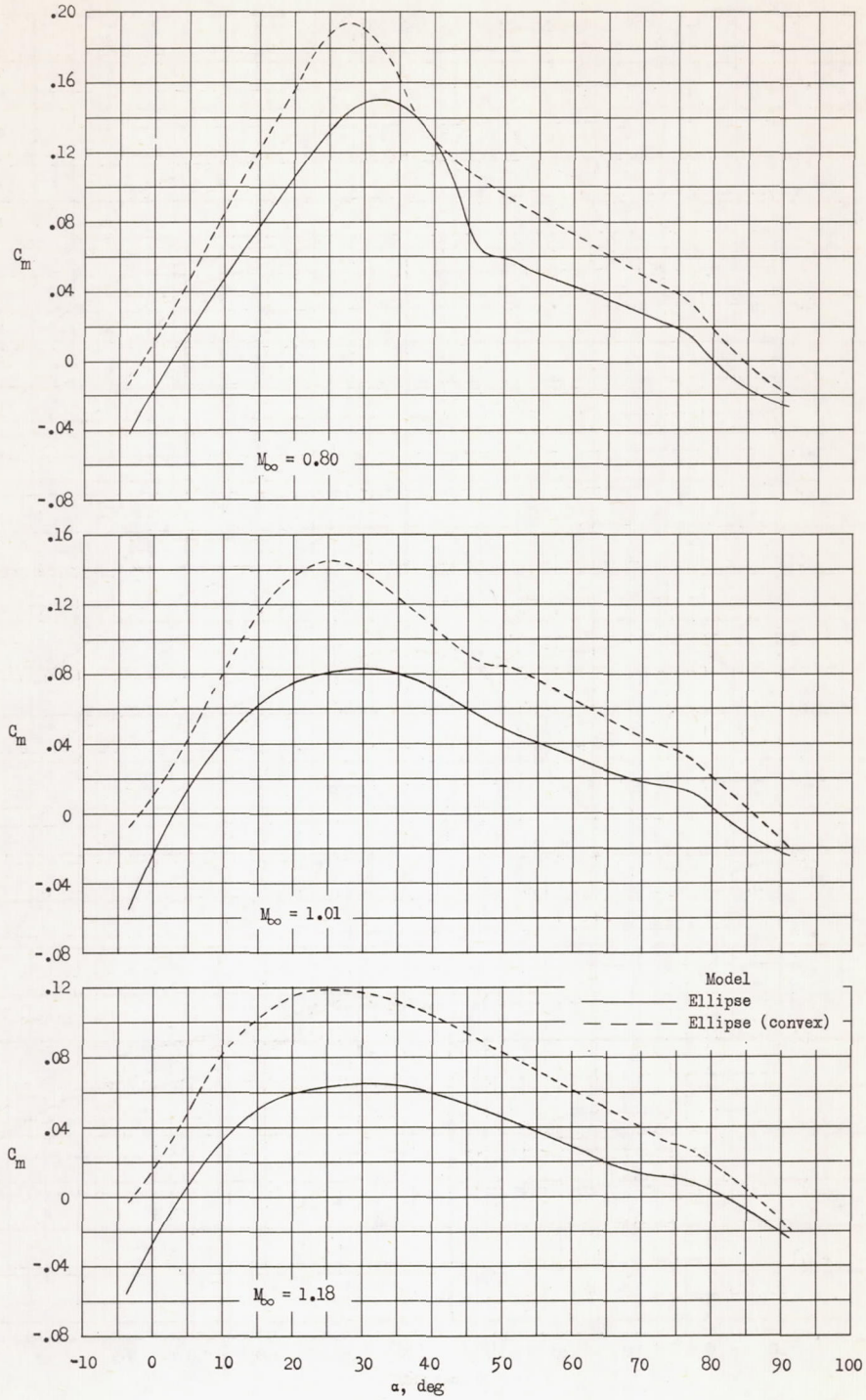


(c) Lower surface contour, ellipse model.

Figure 17.- Continued.

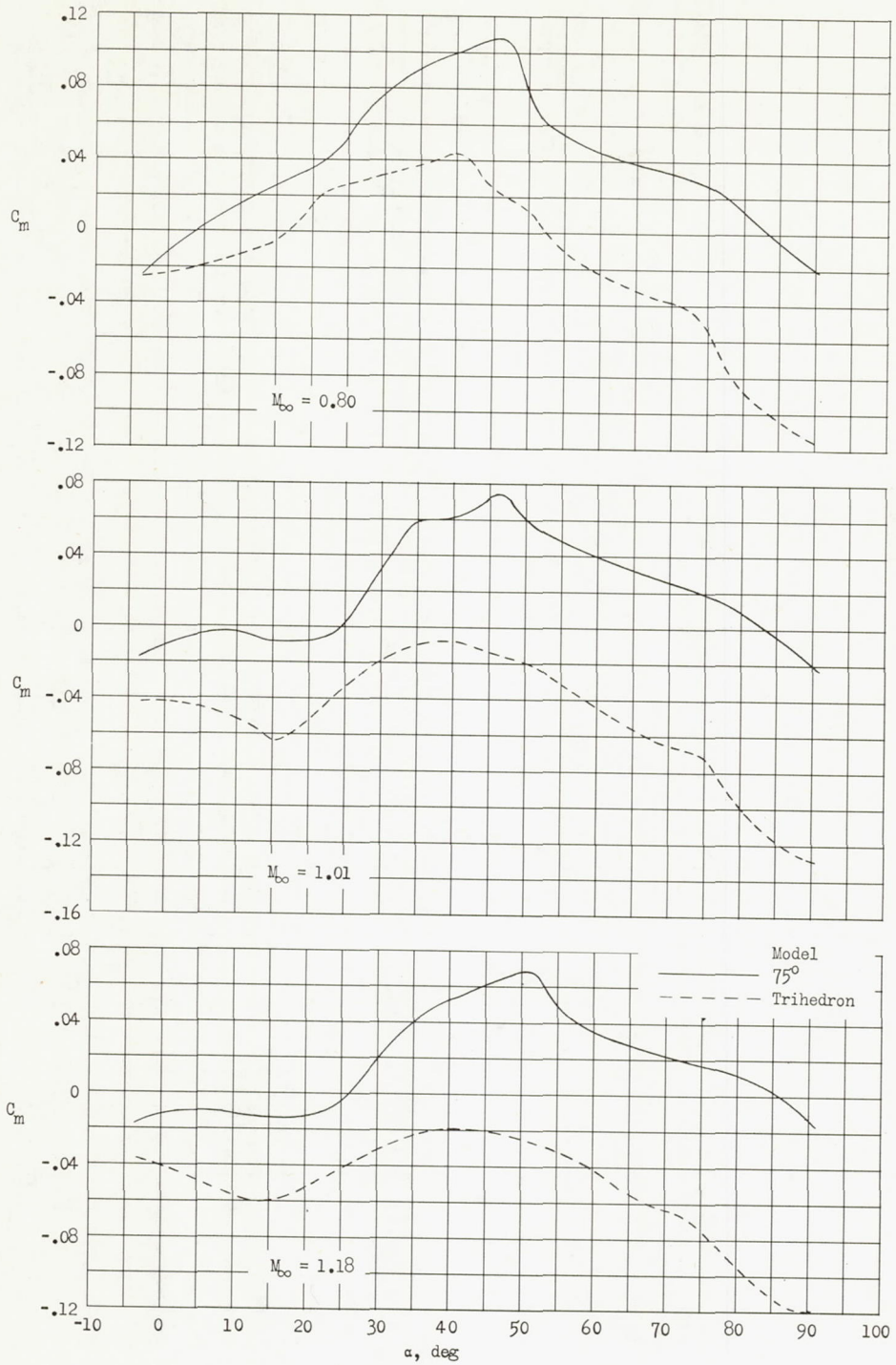


(d) Lower surface contour, 75° model.

Figure 17.- Concluded.



NASA-Langley, 1963 L-1894